PHILOSOPHICAL TRANSACTIONS OF THE ROYAL SOCIETY A MATHEMATICAL, PHYSICAL & ENGINEERING SCIENCES

On the Mechanics of Submerged Vertical Slender Structures Subjected to Varying Axial Tension

M. H. Patel and M. A. Vaz

Phil. Trans. R. Soc. Lond. A 1996 **354**, 609-648
doi: 10.1098/rsta.1996.0021

On the mechanics of submerged vertical slender structures subjected to varying axial tension

By M. H. Patel and M. A. Vaz†

Santa Fe Laboratory for Offshore Engineering, Department of Mechanical Engineering, University College London, Torrington Place, London WC1E 7JE, UK

Contents

		PAGE
1.	Introduction	610
2.	Initial post-buckling behaviour	614
	(*a*) First-order solution	616
	(*b*) Second-order solution	616
	(*c*) Combined full solution	618
3.	Forced lateral excitations	619
4.	Results and discussion	622
5.	Conclusions	642
	Appendix A. Curvature and end shortening	643
	Appendix B. Calculating the point of maximum displacement	643
	Appendix C. Deriving the second-order governing equation	644
	Appendix D. Calculating bending moment and stress	645
	Appendix E. Determination of the equivalent linear damping	646
	References	646

This paper presents a mathematical basis for determining the structural and hydroelastic behaviour of submerged vertical slender steel structures operating at low tension. These structures have significant bending stiffness combined with significant self-weight so that the axial force varies greatly from one end to the other and may even change sign. Such structures form key components of drilling and production platforms used for exploitation of hydrocarbons under the world's oceans. An understanding of their structural behaviour under reduced tension offers opportunities for cost reduction and further optimization. The buckling behaviour at low tension is evaluated by retaining nonlinear curvature terms and using an expansion in series to reduce the governing equation to a set of linear ordinary differential equations, which are then solved sequentially by employing Galerkin's technique. This approach is also extended to lateral oscillation of the structure when excited by forced horizontal oscillatory motions at the top end. The paper uses these solution techniques to explore the behaviour at low tension of typical slender structures used in offshore developments.

† Present address: Laboratory for Submarine Technology, Federal University of Rio de Janeiro, Brazil.

Phil. Trans. R. Soc. Lond. A (1996) **354**, 609–648
Printed in Great Britain

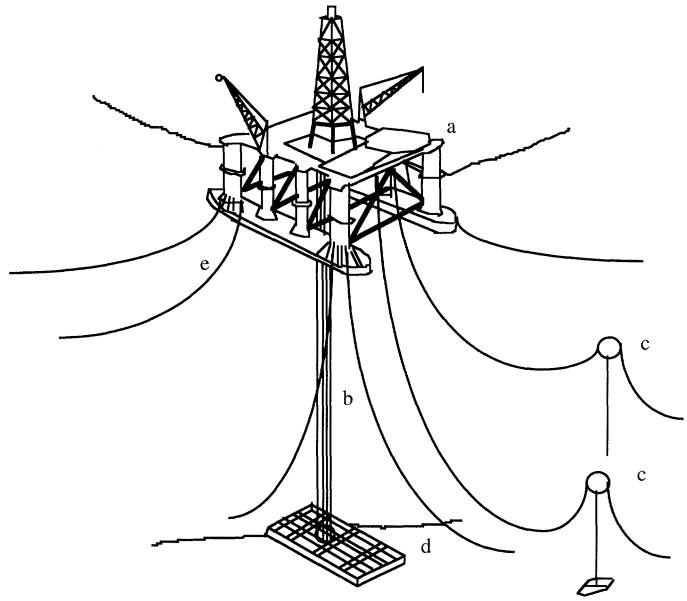

Figure 1. (*a*) Typical semisubmersible with vertical marine riser system: a, surface platform; b, multitube vertical drilling and production riser; c, flexible production risers; d, seabed template; e, catenary moorings.

1. Introduction

Slender vertical steel structures are used in offshore oil and gas platforms, either as so-called 'riser pipes' connecting floating platforms to seabed well heads, as drill strings employed to drill oil wells or as the mooring tethers of tensioned buoyant platforms (TBPs). Due to the pipe self-weight, the axial force may vary considerably from one end to the other. This feature needs to be taken into account when analysing such structures.

Riser pipes range in external diameter from 150 mm to 915 mm and are routinely used in lengths ranging from 50 m up to 1500 m, although considerably greater lengths have been employed for geophysical investigative drilling. These pipes have to be maintained in tension to prevent buckling, although for deployment in deep water the required tension is reduced by buoyancy compartments along the riser structure. There are, therefore, several operational advantages to be gained from the ability to use lower tension for these riser structures. Figure 1*a* gives a schematic of a marine riser operating from a floating platform.

Another class of similar slender structures used in the oil industry are drill pipes. Drill pipes are used to operate a cutting bit at their lower end with conventional drilling being carried out by rotating the cutting bit in combination with a compressive force applied by the bit against the formation. This compressive load on bit arises from the distributed self-weight of the drill pipes giving a compressive maximum axial force at the bottom to a tensile maximum at the top end.

The vertical mooring tethers of tensioned buoyant platforms (TBPs) are another type of slender submerged structure. TBPs are floating structures where a significant proportion of the surface platform's buoyancy (from 10 to 27%) is reacted by vertical tension from 12 to 16 steel tethers ranging in length from 117 m up to 835 m. Figure 1*b* gives a perspective view of a typical TBP, whereas table 1 presents an overview

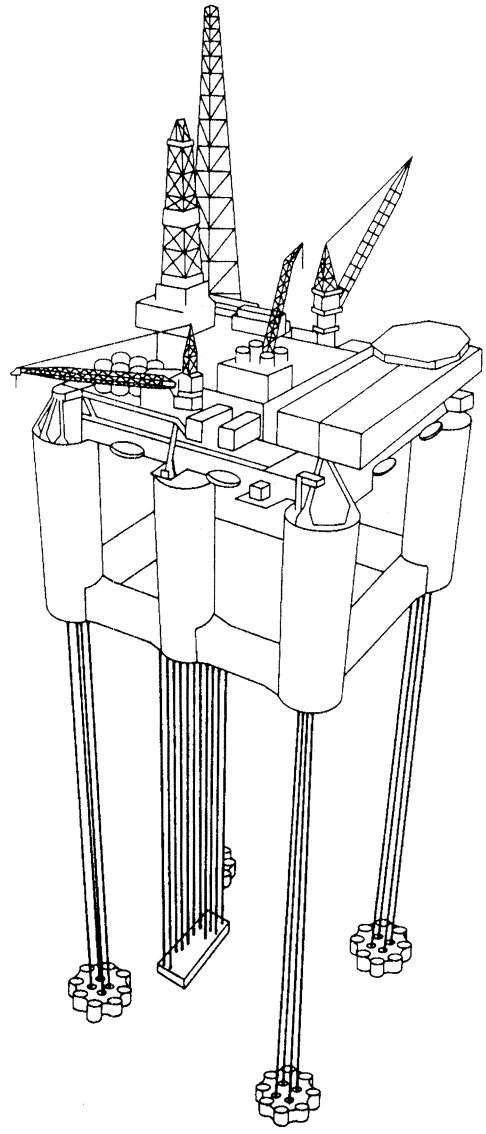

Figure 1. (*b*) Schematic diagram of Hutton TBP.

of the principal particulars of several TBP designs. The vertical mooring tethers of a TBP introduce a design feature which makes the surface platform highly compliant to horizontal surge and sway wave forces and yaw moments. This ensures that the TBP's natural periods in surge, sway and yaw are well above the range of predominant wave periods. At the same time, the vertical tethers introduce high stiffnesses in heave, roll and pitch, which serve to virtually eliminate these modes of motion and also shorten natural periods in these degrees of freedom to be below the periods of predominant wave action.

These characteristic features of the motion of a TBP in waves leads to a number of

Table 1. *Typical design data for tension buoyant platform and tethers*

(Note that the data below are nominal data representative of each of these structures and should not be regarded as exact.)

Parameter	Hutton	Jolliet	Snorre	Auger	Heidrun
year of installation	1984	1989	1992	1993	1995
displacement/t	64 300	16 900	108 200	67 300	296 700
water depth/m	147	536	300	872	345
TBP operational draught/m	33	23	35	37	70
tether length/m	114	573	265	835	275
tether tensions/weight displacement[b]	0.23	0.27	0.27	0.16	0.10
riser tension/weight displacement[a]	0.02	0.09	0.03	0.10	0.02
deck weight/weight displacement[a]	0.36	0.34	0.39	0.40	0.20
column volume/volume displacement[a]	0.70	0.69	0.69	0.69	0.85
WPA/volume displacement/m^{-1}[c]	0.021	0.029	0.018	0.024	0.011
number of tethers per corner	4	3	4	3	3
total number of tethers	16	12	16	12	12
tether OD/m	0.260	0.600	0.810	0.660	1.118
tether ID/m	0.075	0.560	0.734	0.595	1.046
tether wall thickness/mm	92.5	20.0	38	33	36
top tension in single tether[b]/kN	9100	4000	18 500	8800	24 000
tether EI ($\times 10^6$ Nm^2)	46.11	317.6	1424.7	663.1	3711.0
top tension/weight[a]	21.3	2.77	9.82	6.39	9.249
tether CSA/m^2[c]	0.0364	0.0364	0.0922	0.0650	0.1224
tether total weight in air/MN	0.4279	1.442	1.8832	1.378	2.595
tether mean axial stress/MN m^{-2}	187	110	201	135	196

[a]Representative design value which can vary due to tidal and operational conditions.
[b]Non-dimensional units. Some of these data are from Fines (1993).
[c]WPA denotes water plane area, CSA denotes cross sectional area

merits and drawbacks for their use as floating production platforms. The suppression of vertical motion by the tether mooring system provides a stable operating base and simplifies accessibility to seabed well heads and equipment. The tethered nature of the floating platform also makes its cost less sensitive to water depth, and reduces field abandonment costs, although the tether submerged weight needs to be kept as low as possible to maximize deckload capacity. The TBP design allows for fabrication and outfitting to be completed in a construction yard or inshore location prior to installation. Set against these advantages are the drawbacks of the TBP, which requires foundations capable of withstanding large upward forces, coupled with the fact that high tether stresses require careful design and maintenance of these components. A TBP is also more sensitive to mass distribution changes and has significant operational limits on total payload.

One approach to reducing the high cost of TBP-based developments is to evolve the platform and tether design towards an operating state, where the tethers are permitted to go to low and even compressive tensions for part of the cycle of extreme ocean waves. However, an investigation of the feasibility of this requires methods for

PHILOSOPHICAL TRANSACTIONS OF THE ROYAL SOCIETY A MATHEMATICAL, PHYSICAL & ENGINEERING SCIENCES

evaluating and understanding the post-buckling behaviour of TBP tethers. This paper presents work carried out towards achieving this understanding.

A brief literature survey of analysis methods and design techniques used to date in marine risers is presented as a prelude to the rest of the paper. Morgan (1974, 1975, 1976) presents an interesting description of the historical development of marine riser technology and describes all the fundamental features that govern vertical steel riser design and selection. Most analysis work on steel risers has been carried out to determine lateral motions and corresponding stresses due to forces induced by ocean currents, waves and surface vessel motions. Gardner & Kotch (1976), Sparks (1979), Patel *et al.* (1984), McIver & Lunn (1983), Malahy (1986) and Wang (1983) present some typical analysis methods. The role of internal and external hydrostatic pressure in modifying the governing equations of motions was first identified by Young & Fowler (1978). The resultant concept of effective tension has now been incorporated generally into design methods for theses structures. Vertical steel risers at high water depths are also susceptible to axial vibrations. These have been investigated by Sparks *et al.* (1983) and Miller & Young (1985).

For the case of TBPs, the pioneering work of Paulling & Horton (1970) and Horton (1975) led to the first sea-going prototype being installed offshore Santa Catalina Island, California in 1975 by Deep Oil Technology Inc. (Paulling & Horton 1975; Annon 1975). The platform was installed in 61 m of water and tests were carried out in a variety of sea states in 1975 and 1978. Two similar moored platform designs were also developed and small-scale test structures were installed in offshore locations. MacDonald (1974) describes the installation of a 120 ft fully restrained (in all six degrees of freedom) moored structure off the west coast of Scotland between 1963 and 1965. A design similar to that of a TBP was installed in the 1960s by Mitsubishi Heavy Industries of Japan. Since then, a large number of engineering and analytical investigations have been carried out on TBP designs (Perret & Webb 1980; Addison & Steinsvik 1976; Robren & Steinsvik 1977; Natvig & Pendered 1977; Albrecht *et al.* 1978; Capanoglu 1979; Lonergen 1979, 1980; Kitami *et al.* 1982; Tassinin & Panuzzolo 1981).

All of these studies culminated in the decision by Conoco in 1979 to build the first production TBP for drilling and production of hydrocarbons—the site being the North Sea Block 211/27, known as Hutton, with a water depth of 147 m. This TBP, known as the Conoco Hutton Platform, is described by Mercier (1982). It is shown schematically in figure 1*b* with its principal particulars listed in table 1. It produced its first oil in August 1984. Since that time, a succession of TBPs have been installed on the Jolliet, Snorre, Auger and Heidrun fields, together with planned installations such as that on the Mars field in the Gulf of Mexico. Following the installation of the first two TBPs, the phenomenon of springing and transient ringing axial vibrations in TBP tethers due to nonlinear wave excitations has also been observed. Ringing is a phenomenon associated with large-crested near-breaking wave events. Rainey & Smith (1993) review the slender-body theory and compare it with a second-order diffraction theory. They also review the limitations of existing formulations. Jefferys & Rainey (1994) describe a theory for the ringing phenomenon and use experimental and full-scale data to get an insight into the physics of the response. Slender-body theory is invoked to explain the loading terms which are at least cubic in the wave height. Davies *et al.* (1994) review measured model test responses of a monotower gravity base structure and a TBP to draw conclusions on the nature of loads causing ringing. Simple guidelines for minimizing ringing responses are suggested.

PHILOSOPHICAL TRANSACTIONS OF THE ROYAL SOCIETY A MATHEMATICAL, PHYSICAL & ENGINEERING SCIENCES

Now, in order to explore the feasibility of utilizing lower tensions in marine risers and TBP tethers, it is necessary to determine the post-buckling behaviour of these structures with due account of the large deflection nonlinearity in the problem. It needs to be pointed out that, in the case of TBPs, the behaviour of tethers at low tension will feed back into the restoring forces applied on the platform and its natural periods of the platform, particularly for surge, sway and yaw. This interaction of the low-tension tether with the surface platform is not considered here and is the subject of current research.

2. Initial post-buckling behaviour

This part of the paper considers a slender vertical structure's response to reducing axial tension at its upper end. Figure 2 shows a definition diagram for the structure terminated at its end points by ball joints or hinges. The non-dimensionalizing of the governing equation's principal physical variables leads to compact mathematical notation and the opportunity to compare parameters across different TBP tether, marine riser and drill pipe structures.

The material of the structure is assumed elastic and homogeneous, and axial stretching and shear deformations are neglected. The buckled structure is represented by a function $W(X)$. The governing equation—referred to the Lagrangian coordinate system of figure 2—is then expressed as

$$EI\frac{\mathrm{d}^2}{\mathrm{d}X^2}\left[\frac{\mathrm{d}^2W}{\mathrm{d}X^2}\Big/\sqrt{1-\left(\frac{\mathrm{d}W}{\mathrm{d}X}\right)^2}\right]+p(X_2-X)\frac{\mathrm{d}^2W}{\mathrm{d}X^2}-p\frac{\mathrm{d}W}{\mathrm{d}X}=0, \tag{2.1}$$

where E is Young's modulus, I is the second moment of the cross-sectional area, p is the slender structure's 'effective' weight in water per unit length, and X_2 is the longitudinal coordinate of the neutral point. The neutral point is here defined as the point of zero effective axial tension. In normal operating conditions, the tether is fully taut and $X_2 < 0$. However, as the tether pre-tension decreases, the neutral point moves upward. Appendix A gives the curvature and end shortening as functions of the Cartesian coordinates.

It has been shown originally by Young & Fowler (1978) and extended by Sparks (1979) and Seyed & Patel (1992) that the coefficient multiplying the second derivative in equation (2.1) is an 'effective' tension term written as $(T+p_\mathrm{o}A_\mathrm{o}-p_\mathrm{i}A_\mathrm{i})$, where T is the physical tension, p_o and p_i are the external and internal fluid pressures acting on the tubular slender structure, and A_o and A_i are the areas of cross section of the whole pipe and of the inner bore, respectively. This 'effective tension' term takes account of hydrostatic pressure-induced forces which combine with pipe curvature to produce a lateral force analogous to tension on the pipe body.

For a specific tether, riser pipe or drill pipe, equating $p(X_2-X)$ with $(T+p_\mathrm{o}A_\mathrm{o}-p_\mathrm{i}A_\mathrm{i})$ will enable the resultant values of p and X_2 to be used in equation (2.1), taking full account of the hydrostatic pressure and curvature-induced terms. However, the formulation of equation (2.1) is kept in terms of the $p(X_2-X)$ term multiplying the second derivative so as to simplify the presentation of the later analysis.

Equation (2.1) can be made non-dimensional by using the following relations: $EI=pm^3$, $W=mw$, $X=mx$ and $X_2=mx_2$. This results in

$$\left[\frac{w''}{\sqrt{1-w'^2}}\right]''+(x_2-x)w''-w'=0, \tag{2.2}$$

PHILOSOPHICAL TRANSACTIONS OF THE ROYAL SOCIETY A MATHEMATICAL, PHYSICAL & ENGINEERING SCIENCES

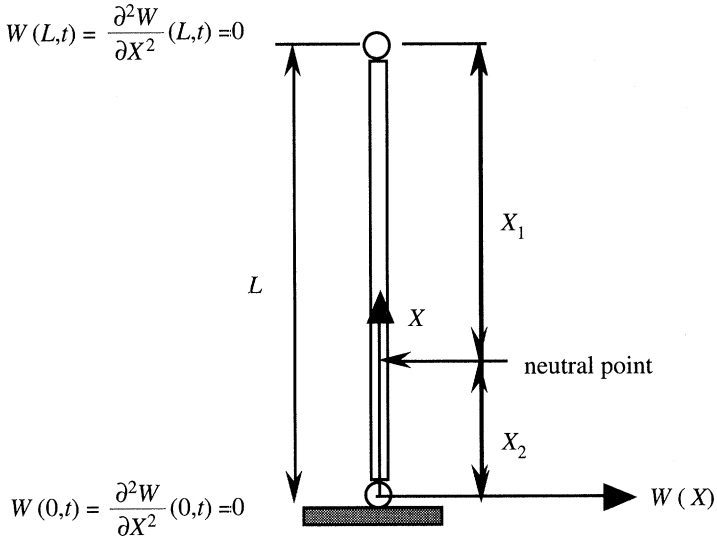

Figure 2. Schematic of a uniform slender structure.

where the symbol $'$ denotes differentiation with respect to x. Differentiating the first term of equation (2.2) twice, expanding it in a Taylor series and only retaining terms up to second order, gives

$$w''''(1+\tfrac{1}{2}w'^2)+(w''^3+3w'w''w''')+(x_2-x)w''-w'=0. \tag{2.3}$$

This approach has been applied previously by El Naschie (1990) to the case of a bar with uniform axial force, whereas the development here is aimed at deriving results for a variable axial force.

The non-dimensional deflection $w(x)$ and the non-dimensional load on the lower ball joint x_2 are taken to be a series of the form

$$w(x)=w_0(x)+\zeta w_1(x)+\zeta^2 w_2(x)+\zeta^3 w_3(x)+\cdots, \tag{2.4a}$$

$$x_2=x_2^{(0)}+\zeta x_2^{(1)}+\zeta^2 x_2^{(2)}+\zeta^3 x_2^{(3)}+\cdots, \tag{2.4b}$$

where ζ is a perturbation parameter—defined as the maximum displacement of the buckled structure. However, due to the symmetry of the problem, $w(x)$ should be odd and x_2 even. Then,

$$w(x)=\zeta w_1(x)+\zeta^3 w_3(x)+\cdots, \tag{2.4c}$$

$$x_2=x_2^{(0)}+\zeta^2 x_2^{(2)}+\cdots. \tag{2.4d}$$

Now substituting equations (2.4 *c*) and (2.4 *d*) in (2.3) gives

$$\Big(\sum_i \zeta^i w_i''''\Big)\Big(1+\tfrac{1}{2}\sum_i\sum_j \zeta^i\zeta^j w_i'w_j'\Big)-\Big(\sum_i \zeta^i(xw_i''+w_i')\Big)$$
$$+\Big(\sum_i\sum_j\sum_k \zeta^i\zeta^j\zeta^k(3w_i'w_k'''+w_i''w_k'')w_j''\Big)+\Big(\sum_n\sum_i \zeta^n\zeta^i x_2^{(n)}w_i''\Big)=0, \tag{2.5}$$

where i,j,k are odd and n is $0,2,4,\ldots$, and so on. Separating terms proportional to

ζ and ζ^3, respectively, results in

$$w_1'''' + (x_2^{(0)} - x)w_1'' - w_1' = 0, \tag{2.6a}$$

$$w_3'''' + (x_2^{(0)} - x)w_3'' - w_3' = -(\tfrac{1}{2}w_1''''w_1'^2 + 3w_1'w_1''w_1''' + w_1''^3 + x_2^{(2)}w_1''). \tag{2.6b}$$

The linear equations (2.6) can be solved sequentially: solution of equation (2.6 *a*) gives $w_1(x)$, which can then be substituted in equation (2.6 *b*) to obtain $w_3(x)$. In this work, a Galerkin approximation method is used for this.

(*a*) *First-order solution*

The first-order solution $w_1(x)$ can be approximated by the following equation:

$$w_1(x) = \sum_{n=1}^{N} a_n \sin(n\pi x/l), \tag{2.7a}$$

where L is the structure's physical length with a corresponding non-dimensional length l, given by $L = ml$. Note that equation (2.7 *a*) automatically satisfies the pinned or hinged boundary conditions at both ends. Then, substituting equation (2.7 *a*) into (2.6 *a*), multiplying it by $\sin(k\pi x/l)$ and integrating from $x = 0$ to $x = l$ produces

$$\sum_{n=1}^{N} \left\{ \tfrac{1}{2}l[(k\pi/l)^4 + (\tfrac{1}{2}l - x_2^{(0)})(k\pi/l)^2]a_k - \frac{2nk(n^2+k^2)}{(n^2-k^2)^2}a_n \right\} = 0. \tag{2.7b}$$

Equation (2.7 *b*) expresses a system of simultaneous linear equations admitting a non-trivial solution only if the determinant vanishes. The equations can also be written as

$$[M]\{a\} = \{0\}. \tag{2.7c}$$

Solution of equation (2.7 *b*) gives $x_2^{(0)}$ and eigenvectors $\{a_n\}$. However, at the point of maximum displacement, $x = \tilde{x}$, $w_1'(\tilde{x}) = 0$ and $w_1(\tilde{x})$. Hence, these conditions lead to

$$\sum_{n=1}^{N} a_n(n\pi/l)\cos(n\pi\tilde{x}/l) = 0 \tag{2.8a}$$

and

$$\sum_{n=1}^{N} a_n \sin(n\pi\tilde{x}/l) = 1. \tag{2.8b}$$

The point of maximum displacement can be determined from equation (2.8 *a*) (see Appendix B) and, hence, the vector $\{a\}$ can be obtained from equation (2.8 *b*).

(*b*) *Second-order solution*

Turning our attention to the second-order solution, substituting equation (2.7 *a*) into (2.6 *b*) gives

$$w_3'''' + (x_2^{(0)} - x)w_3'' - w_3'$$
$$= -\tfrac{1}{2}(\pi/l)^6 \sum_{i=1}^{N}\sum_{j=1}^{N}\sum_{k=1}^{N} a_i a_j a_k i^4 jk \sin(i\pi x/l)\cos(j\pi x/l)\cos(k\pi x/l)$$

$$-3(\pi/l)^6 \sum_{i=1}^{N}\sum_{j=1}^{N}\sum_{k=1}^{N} a_i a_j a_k ij^2k^3 \cos(i\pi x/l)\sin(j\pi x/l)\cos(k\pi x/l)$$

$$+(\pi/l)^6 \sum_{i=1}^{N}\sum_{j=1}^{N}\sum_{k=1}^{N} a_i a_j a_k i^2j^2k^2 \sin(i\pi x/l)\sin(j\pi x/l)\sin(k\pi x/l)$$

$$+x_2^{(2)}(\pi/l)^2 \sum_{i=1}^{N} a_i i^2 \sin(i\pi x/l), \tag{2.9 a}$$

and simplifying the right-hand side of equation (2.9 *a*) (see Appendix C) results in

$$w_3'''' + (x_2^{(0)} - x)w_3'' - w_3' = \sum_{i=1}^{N}[C_i + x_2^{(2)}\bar{a}_i]\sin(i\pi x/l) + \sum_{i=N+1}^{3N} C_i \sin(i\pi x/l), \tag{2.9 b}$$

where the coefficients C_i and $\bar{a}_i$ are defined in Appendix C.

Equation (2.9 *b*) is a fourth-order ordinary linear equation, which can be solved in the following way:

(1) determine the homogeneous solution $w_3^{(0)}(x)$ from

$$w_3'''' + (x_2^{(0)} - x)w_3'' - w_3' = 0; \tag{2.10 a}$$

(2) determine the first particular solution $w_3^{(1)}(x)$ from

$$w_3'''' + (x_2^{(0)} - x)w_3'' - w_3' = \sum_{i=1}^{N}[C_i + x_2^{(2)}\bar{a}_i]\sin(i\pi x/l); \tag{2.10 b}$$

(3) determine the second particular solution $w_3^{(2)}(x)$ from

$$w_3'''' + (x_2^{(0)} - x)w_3'' - w_3' = \sum_{i=N+1}^{3N} C_i \sin(i\pi x/l); \tag{2.10 c}$$

(4) add $w_3^{(0)}(x) + w_3^{(1)}(x) + w_3^{(2)}(x)$ to obtain $w_3(x)$.

Equation (2.10 *a*), similar to (2.6 *a*), is also solved by Galerkin's method. The solution is approximated by

$$w_3^{(0)}(x) = \sum_{n=1}^{N} b_n \sin(n\pi x/l),$$

then $\{b_n\} = \{a_m\}$. Hence,

$$\sum_{n=1}^{N}\left\{\tfrac{1}{2}l[(k\pi/l)^4 + (\tfrac{1}{2}l - x_2^{(0)})(k\pi/l)^2]b_k - \frac{2nk(n^2+k^2)}{(n^2-k^2)^2}b_n\right\} = 0, \tag{2.11 a}$$

and equation (2.11 *a*) can also be written as

$$[M]\{b\} = \{0\}. \tag{2.11 b}$$

The first particular solution is also written in terms of a trigonometric series as

$$w_3^{(1)}(x) = \sum_{n=1}^{N} e_n \sin(n\pi x/l).$$

Galerkin's method is used again to give

$$\sum_{n,k=1}^{N}\left\{\tfrac{1}{2}l[(k\pi/l)^4+(\tfrac{1}{2}l-x_2^{(0)})(k\pi/l)^2]e_k-\frac{2nk(n^2+k^2)}{(n^2-k^2)^2}e_n\right\}=\tfrac{1}{2}[C_k+x_2^{(2)}\bar{a}_k]l, \tag{2.11 c}$$

or

$$[M]\{e\}=\tfrac{1}{2}l[\{C\}+x_2^{(2)}\{\bar{a}\}]. \tag{2.11 d}$$

In a similar way, the second particular solution is written in terms of trigonometric series as

$$w_3^{(2)}(x)=\sum_{n=N+1}^{3N}d_n\sin(n\pi x/l),$$

and Galerkin's method is employed to obtain

$$\sum_{n,k=N+1}^{N}\left\{\tfrac{1}{2}l[(k\pi/l)^4+(\tfrac{1}{2}l-x_2^{(0)})(k\pi/l)^2]d_k-\frac{2nk(n^2+k^2)}{(n^2-k^2)^2}d_n\right\}=\tfrac{1}{2}lC_k. \tag{2.11 e}$$

(c) *Combined full solution*

Now the solutions of equations (2.10 *a*)–(2.10 *c*) are combined to give

$$w_3(x)=\sum_{n=1}^{N}\bar{b}_n\sin(n\pi x/l)+\sum_{n=N+1}^{3N}d_n\sin(n\pi x/l), \tag{2.12}$$

where $\bar{b}_n=b_n+e_n$. However, at the point of maximum displacement, $w_3(\tilde{x})=0$, so that

$$\sum_{n=1}^{N}\bar{b}_n\sin(n\pi\tilde{x}/l)=-\sum_{n=N+1}^{3N}d_n\sin(n\pi\tilde{x}/l)=C_{N+1}. \tag{2.13 a}$$

Adding equation (2.11 *b*) to (2.11 *d*) gives

$$[M]\{\bar{b}\}=\tfrac{1}{2}l[\{C\}+x_2^{(2)}\{\bar{a}\}], \tag{2.13 b}$$

and combining equation (2.13 *a*) with (2.13 *b*) produces

$$\left.\begin{aligned}
M_{11}\bar{b}_1+M_{12}\bar{b}_2+\cdots+M_{1N}\bar{b}_N-\tfrac{1}{2}l\bar{a}_1x_2^{(2)}&=\tfrac{1}{2}lC_1,\\
M_{21}\bar{b}_1+M_{22}\bar{b}_2+\cdots+M_{2N}\bar{b}_N-\tfrac{1}{2}l\bar{a}_2x_2^{(2)}&=\tfrac{1}{2}lC_2,\\
\vdots\qquad\quad\vdots\qquad\quad\vdots\qquad\quad\vdots\qquad\quad\vdots&\\
M_{N1}\bar{b}_1+M_{N2}\bar{b}_2+\cdots+M_{NN}\bar{b}_N-\tfrac{1}{2}l\bar{a}_Nx_2^{(2)}&=\tfrac{1}{2}lC_N,\\
\sin(\pi\tilde{x}/l)\bar{b}_1+\sin(2\pi\tilde{x}/l)\bar{b}_2+\cdots+\sin(N\pi\tilde{x}/l)\bar{b}_N+0x_2^{(2)}&=C_{N+1}.
\end{aligned}\right\} \tag{2.14}$$

Equation (2.14) consists of $N+1$ variables ($\bar{b}_n$ and $x_2^{(2)}$) and $N+1$ equations, which can be readily solved. Note that the bending moment $M(x)$ is given by

$$M(x)=EI\frac{W''}{\sqrt{1-W'^2}}=pm^2w''(1+\tfrac{1}{2}w'^2). \tag{2.15 a}$$

Substituting equation (2.4 *c*) into (2.15 *a*) and retaining terms up to second order gives

$$M(x)=pm^2[\zeta w_1''+\zeta^3(w_3''+0.5w_1'^2w_1'')]. \tag{2.15 b}$$

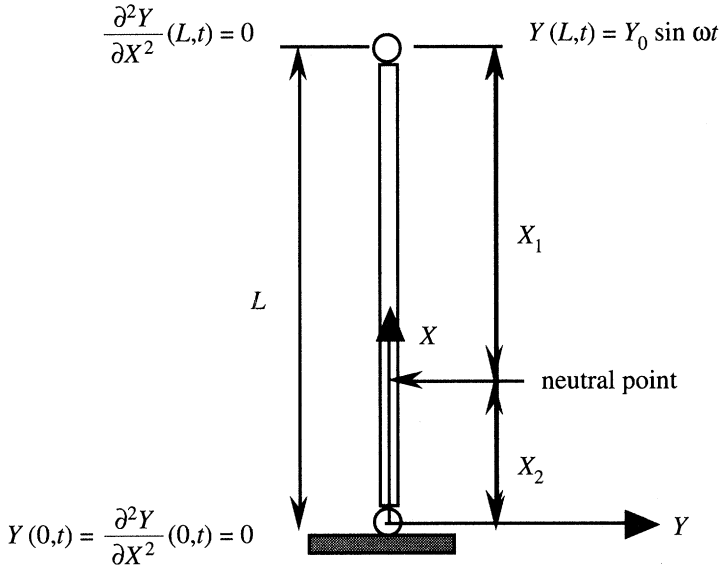

Figure 3. System of reference for a TLP tether.

The non-dimensional bending moment $\bar{m}(x)$ (see Appendix D) is defined as $\bar{m}(x) = M(x)/pm^2$. Furthermore, the buckled shape is calculated by the following equation

$$w(x) = \sqrt{\frac{x_2 - x_2^{(0)}}{x_2^{(2)}}} \left[w_1(x) + \frac{x_2 - x_2^{(0)}}{x_2^{(2)}} w_3(x) \right], \tag{2.16}$$

where

$$\zeta = \sqrt{\frac{x_2 - x_2^{(0)}}{x_2^{(2)}}},$$

$w_1(x)$ and $w_3(x)$ are given by equations (2.7 *a*) and (2.12), respectively.

Results from this analysis are presented in § 4.

3. Forced lateral excitations

In the analysis presented here, forced excitation of the vertical slender structure is assumed to be exclusively due to translational horizontal motions (sway/surge) of the surface platform with the effects of wave and current induced excitations neglected. Figure 3 gives the reference axis system of a TBP tether and its boundary conditions. The main assumptions when deriving the governing equations are that axial deformation is not considered, the tether is a uniform cylinder of a homogeneous elastic material, the axial tension does not vary with time, the resultant deflections and rotations are small and the tether deformation is in one plane only. The governing equation then is

$$EI\frac{\partial^4 Y}{\partial X^4} + p(X_2 - X)\frac{\partial^2 Y}{\partial X^2} - p\frac{\partial Y}{\partial X} + \bar{\rho}\frac{\partial^2 Y}{\partial t^2} + B_{nl}\left|\frac{\partial Y}{\partial t}\right|\frac{\partial Y}{\partial t} = 0, \tag{3.1}$$

where $Y(X,t)$ is a function describing the tether lateral displacement, E is Young's modulus, I is the second moment of area of the cross section, p is the tether effective weight per unit length, X_2 is the longitudinal coordinate of the neutral point, $\bar{\rho}$ is the tether physical plus added mass per unit length and B_{nl} is the quadratic damping constant.

Parameters p and X_2 in this equation include the effects of external and internal hydrostatic pressure and curvature as described earlier for equation (2.1).

The added mass per unit length is given by $\rho C_{\mathrm{m}} A$, where ρ is sea water density, C_{m} is the added mass coefficient and A is the cross-sectional area. Furthermore, the quadratic damping constant is given by $B_{nl} = \frac{1}{2}\rho D C_{\mathrm{D}}$, where D is the tether outside diameter and C_{D} is the drag coefficient which, is approximately 1.2 for typical Keulegan–Carpenter numbers encountered by these slender structures. This formulation of the equation also takes account of the tether 'effective' tension term and its buoyancy forces in sea water in a similar manner to that in § 2.

Equation (3.1) can be non-dimensionalized by using the following relationships:

$$EI = pm^3, \quad \zeta = \bar{\rho} m/p, \quad b_{nl} = B_{nl} m^2/p, \quad X = mx, \quad Y = my, \quad X_2 = mx_2, \tag{3.2}$$

where ζ and b_{nl} are non-dimensional mass and damping parameters, respectively. Note that m is a 'measure' of the relative importance of bending stiffness and effective weight. Hence,

$$\frac{\partial^4 y}{\partial x^4} + (x_2 - x)\frac{\partial^2 y}{\partial x^2} - \frac{\partial y}{\partial x} + \zeta \frac{\partial^2 y}{\partial t^2} + b_{nl}\left|\frac{\partial y}{\partial t}\right|\frac{\partial y}{\partial t} = 0. \tag{3.3a}$$

Equation (3.3 *a*) admits a time-domain solution only, due to the nonlinear damping term. Since this is not convenient at the preliminary design stage, equation (3.3 *a*) can be linearized to give

$$\frac{\partial^4 y}{\partial x^4} + (x_2 - x)\frac{\partial^2 y}{\partial x^2} - \frac{\partial y}{\partial x} + \zeta \frac{\partial^2 y}{\partial t^2} + b_l \frac{\partial y}{\partial t} = 0, \tag{3.3b}$$

where b_l is an equivalent damping constant. The relationship between b_l and b_{nl} is obtained by equalling the energy dissipated by an infinitesimal tether element in one cycle (see Appendix E). Solution of equation (3.3 *b*) allows a less cost frequency domain analysis.

The tether resultant deflection can be decomposed into a rigid body motion and a series of sinusoidal functions, respectively, representing the platform motion and the tether elastic response. The solution may then be approximated by

$$y(x,t) = \left\{\left[x + \sum_{n=1}^{N} a_n \sin(n\pi x/l)\right]\sin\omega t + \left[\sum_{n=1}^{N} b_n \sin(n\pi x/l)\right]\cos\omega t + \right\} y_0/l, \tag{3.4}$$

where l is the tether non-dimensional length, ω the circular frequency of the forced motion, a_n and b_n are coefficients to be determined, N is the number of terms considered and y_0 is the top-ball-joint maximum displacement. Note that equation (3.4) satisfies the four boundary conditions assumed in figure 3. Due to the damping term, the tether lateral displacement contains terms in-phase and out-of-phase with the upper-ball-joint motion.

Substituting equation (3.4) in (3.3 *b*) and separating the terms proportional to

'$\sin\omega t$' and '$\cos\omega t$', respectively, results in

$$\sum_{n=1}^{N} a_n\{[(n\pi/l)^4 - (x_2 - x)(n\pi/l)^2 - \bar{\zeta}]\sin(n\pi x/l) - (n\pi/l)\cos(n\pi x/l)\}$$
$$-x\bar{b}_l \sum_{n=1}^{N} b_n \sin(n\pi x/l) = (1 + \bar{\zeta}x), \tag{3.5 a}$$

$$x\bar{b}_l \sum_{n=1}^{N} a_n \sin(n\pi x/l) + \sum_{n=1}^{N} b_n\{[(n\pi/l)^4 - (x_2 - x)(n\pi/l)^2 - \bar{\zeta}]$$
$$\times \sin(n\pi x/l) - (n\pi/l)\cos(n\pi x/l)\} = -\bar{b}_l x^2, \tag{3.5 b}$$

where

$$\bar{\zeta} = \omega^2\zeta, \quad \text{and} \quad \bar{b}_l = \frac{8}{3\pi}\omega^2\frac{y_0}{l}b_{nl},$$

are, respectively, frequency and damping parameters. Multiplying equations (3.5 *a*) and (3.5 *b*) by $\sin k\pi x/l$, and integrating from $x = 0$ to $x = l$ produces

$$\sum_{n=1}^{N}\left\{\tfrac{1}{2}l[(k\pi/l)^4 + (\tfrac{1}{2}l - x_2^{(0)})(k\pi/l)^2 - \bar{\zeta}]a_k - \frac{2nk(n^2+k^2)}{(n^2-k^2)^2}a_n\right\}$$
$$-\tfrac{1}{4}l^2\bar{b}_l \sum_{n=1}^{N}\left[b_k - \frac{16nk}{\pi^2(n^2-k^2)^2}b_n\right] = C_1(k), \tag{3.6 a}$$

$$\tfrac{1}{4}l^2\bar{b}_l \sum_{n=1}^{N}\left[a_k - \frac{16nk}{\pi^2(n^2-k^2)^2}a_n\right]$$
$$+\sum_{n=1}^{N}\left\{\tfrac{1}{2}l[(k\pi/l)^4 + (\tfrac{1}{2}l - x_2^{(0)})(k\pi/l)^2 - \bar{\zeta}]b_k - \frac{2nk(n^2+k^2)}{(n^2-k^2)^2}b_n\right\} = C_2(k), \tag{3.6 b}$$

where $k = 1, 2, \ldots, N$, and for k odd, n is even and vice versa, otherwise $a_n = b_n = 0$.

Furthermore,

$$C_1(k) = \frac{2l}{\pi k_{\text{odd}}} - \frac{\bar{\zeta}l^2}{k\pi}(-1)^k, \quad \text{and} \quad C_2(k) = \frac{l^3}{\pi k}\bar{b}_l\begin{cases} 1 & k \text{ even}, \\ (2/\pi k)^2 - 1 & k \text{ odd}. \end{cases}$$

Equations (3.6 *a*) and (3.6 *b*) express a system of linear equations from which the following can be obtained.

(a) *Tether deflection for static offset.* This is calculated by setting $\bar{b}_l$ and $\bar{\zeta}$ equal to zero. Hence, b_k $(k = 1, 2, \ldots, n)$ is zero and a_k can be obtained from equation (3.6 *a*). The deflected tether shape can then be obtained from equation (3.4).

(b) *Tether restoring force.* Small inclinations are assumed: hence, the restoring force F_R is given by

$$F_R = T_{TOP}\frac{\partial y}{\partial x}(l, t),$$

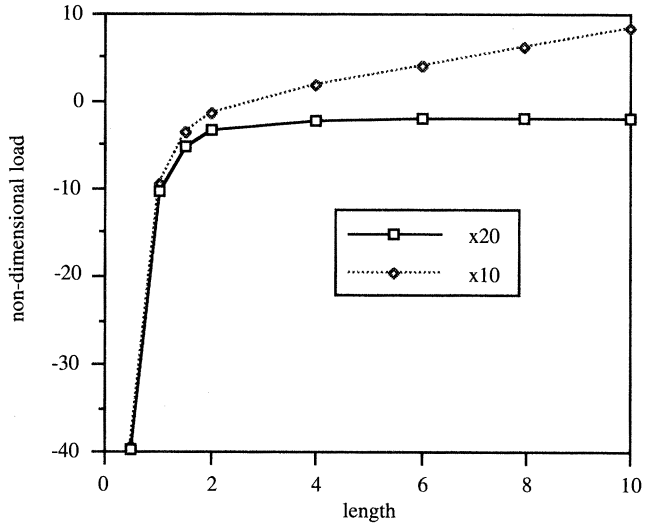

Figure 4. First-order upper and lower buckling loads.

where T_{TOP} is the upper ball joint axial tension. Then

$$F_{\mathrm{R}} = T_{\mathrm{TOP}} \frac{\pi y_0}{l^2} \left\{ \left[\frac{l}{\pi} + \sum_{n=1}^{N} n(-1)^n a_n \right] \sin \omega t + \left[\sum_{n=1}^{N} n(-1)^n b_n \right] \cos \omega t \right\}. \tag{3.7}$$

(c) *Dynamic bending stress.* This is obtained from

$$\sigma_{\mathrm{B}}(x,t) = \tfrac{1}{2} E D \frac{\partial^2 Y}{\partial X^2}(X,t),$$

which reduces to the following equation:

$$\sigma_{\mathrm{B}}(x,t) = -\tfrac{1}{2} E d \frac{\pi^2}{l^3} y_0 \left\{ \left[\sum_{n=1}^{N} n^2 a_n \sin(n\pi x/l) \right] \sin \omega t + \left[\sum_{n=1}^{N} n^2 b_n \sin(n\pi x/l) \right] \cos \omega t \right\}, \tag{3.8}$$

where the non-dimensional tether outside diameter $d = D/m$.

The solution of equations (3.6 *a*) and (3.6 *b*) gives the coefficients a_n and b_n, which can then be substituted into equations (3.4), (3.7) and (3.8) to obtain the lateral deflection, restoring force and bending stress distribution, respectively.

4. Results and discussion

The effects of the theory of §§ 2 and 3 on typical slender structures used in the marine environment are illustrated here by presenting generic results, which retain the non-dimensional variables used in the theory, and then by some more specific case studies.

Initial post buckling behaviour is considered first. For this case, figures 4 and 5 use the solution of equation (2.7 *b*) and equation (2.14) to display variations in the first- and second-order buckling loads at the structure ends as a function of non-dimensional structure length l. Figure 4 presents the buckling loads at the lower ($x_2^{(0)}$) and upper ($x_1^{(0)}$) ends of the structure ($x_1^{(0)} = l - x_2^{(0)}$). Figure 5, on the other

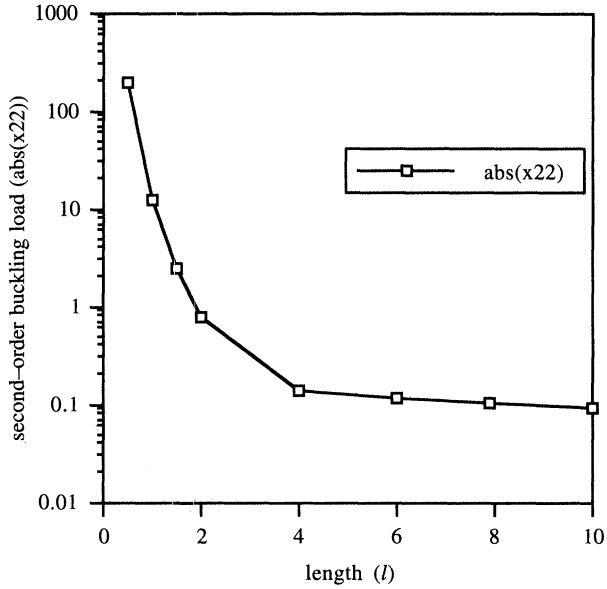

Figure 5. Second-order lower buckling load.

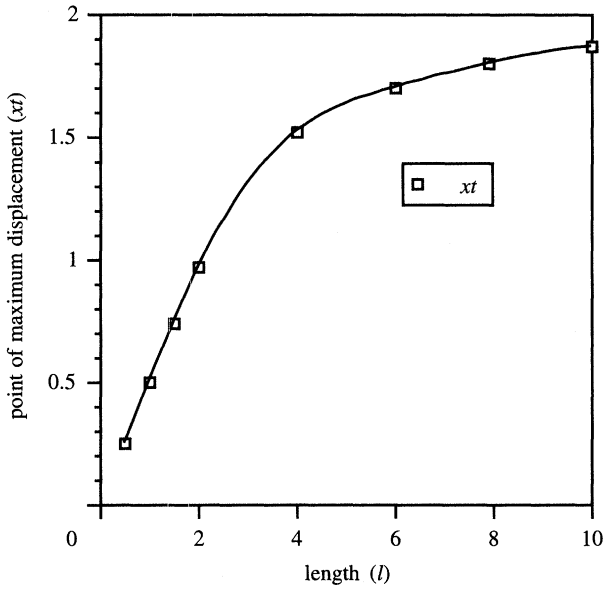

Figure 6. Point of maximum displacement.

hand, presents the non-dimensionalized second-order buckling load ($x_2^{(2)}$)—which is also a function of non-dimensional length l.

The results of figure 4 demonstrate the following.

(1) For $l \cong 2.8$, buckling may occur if the slender structure's weight is fully applied to the lower ball joint.

(2) For $l > 2.8$, the critical buckling load does not depend significantly on the structure's length.

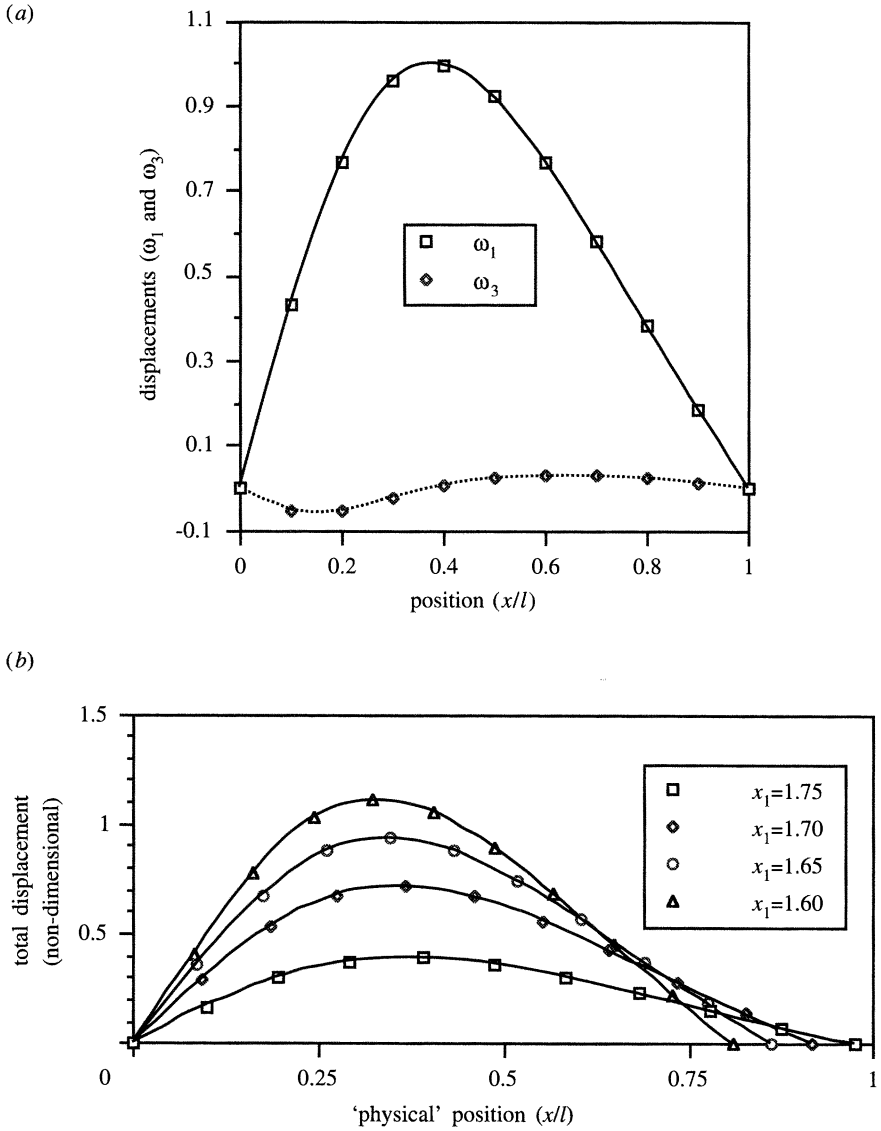

Figure 7. (a) Displacement functions, $l = 4.00$. (b) Lateral displacement.

(3) For $l < 2.8$, a compressive load must be applied to buckle the structure. It is statically stable even if its weight is fully applied to the lower ball joint.

On the other hand, the results of figure 5 show that the second-order component of the buckling load falls off rapidly as the structure length increases. This implies that, for $l > 4$, approximately, the post-buckling behaviour is dominated by increasing lateral displacement governed by the parameter

$$\zeta = \sqrt{\frac{x_2 - x_2^{(0)}}{x_2^{(2)}}}.$$

The point of maximum lateral displacement of the structure $\tilde{x}$ $(= xt)$ is plotted

(*c*)

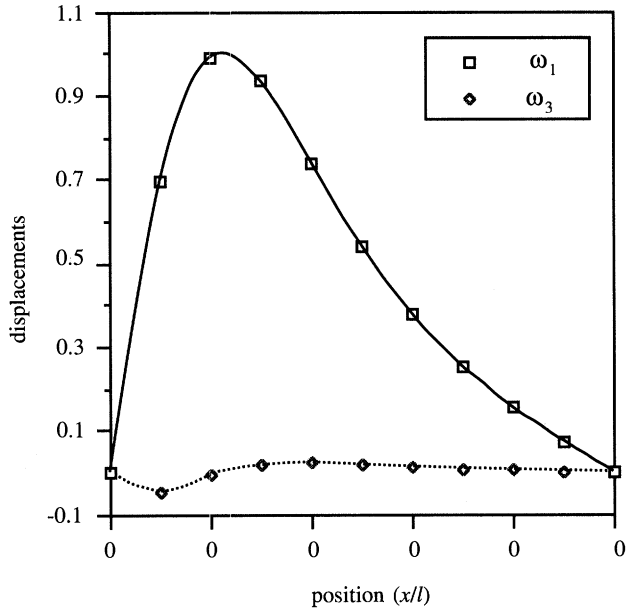

(*d*)

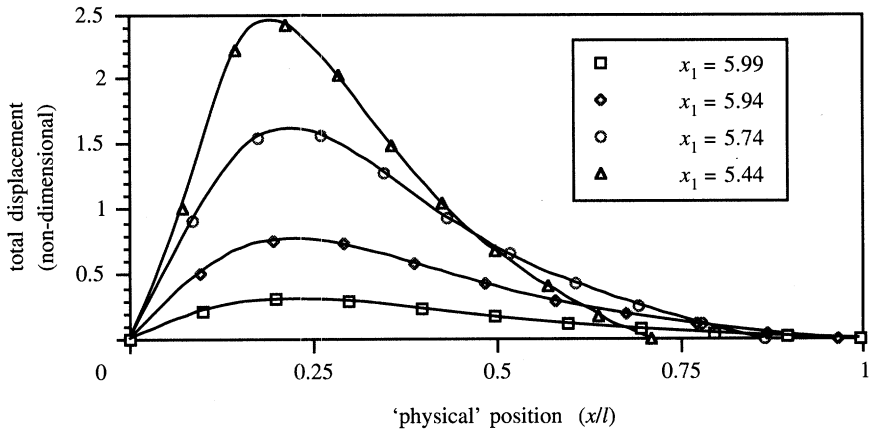

Figure 7. (*c*) Displacement functions, $l = 7.94$. (*d*) Lateral displacement, $x_1^{(0)} = 6.00$, $l = 7.94$.

in figure 6 as a function of non-dimensional length l. This curve results from the solution of equation (2.8 *a*). For $l < 2$, this curve tends asymptotically to $\tilde{x} = 0.5l$, which is the solution for the Euler strut's buckling value. It is also seen that $\tilde{x}$ does not move up the structure's length at the same rate with non-dimensional length. This feature is evident in many numerical computations of marine riser and tether response, but has not been explained previously through an analytical approach.

It was felt to be useful to present some results expressed in terms of physical variables for the first- and second-order displacements $w_1(x)$ and $w_3(x)$. Figures 7*a* and 7*c* present the first- and second-order displacement functions ($w_1(x)$ and $w_3(x)$) for $l = 4$ and $l = 7.94$, respectively. Figures 7*b* and 7*d* (also for $l = 4$ and $l = 7.94$) plot the physical buckled structural displacement as the top tension is decreased. The following two points can be observed.

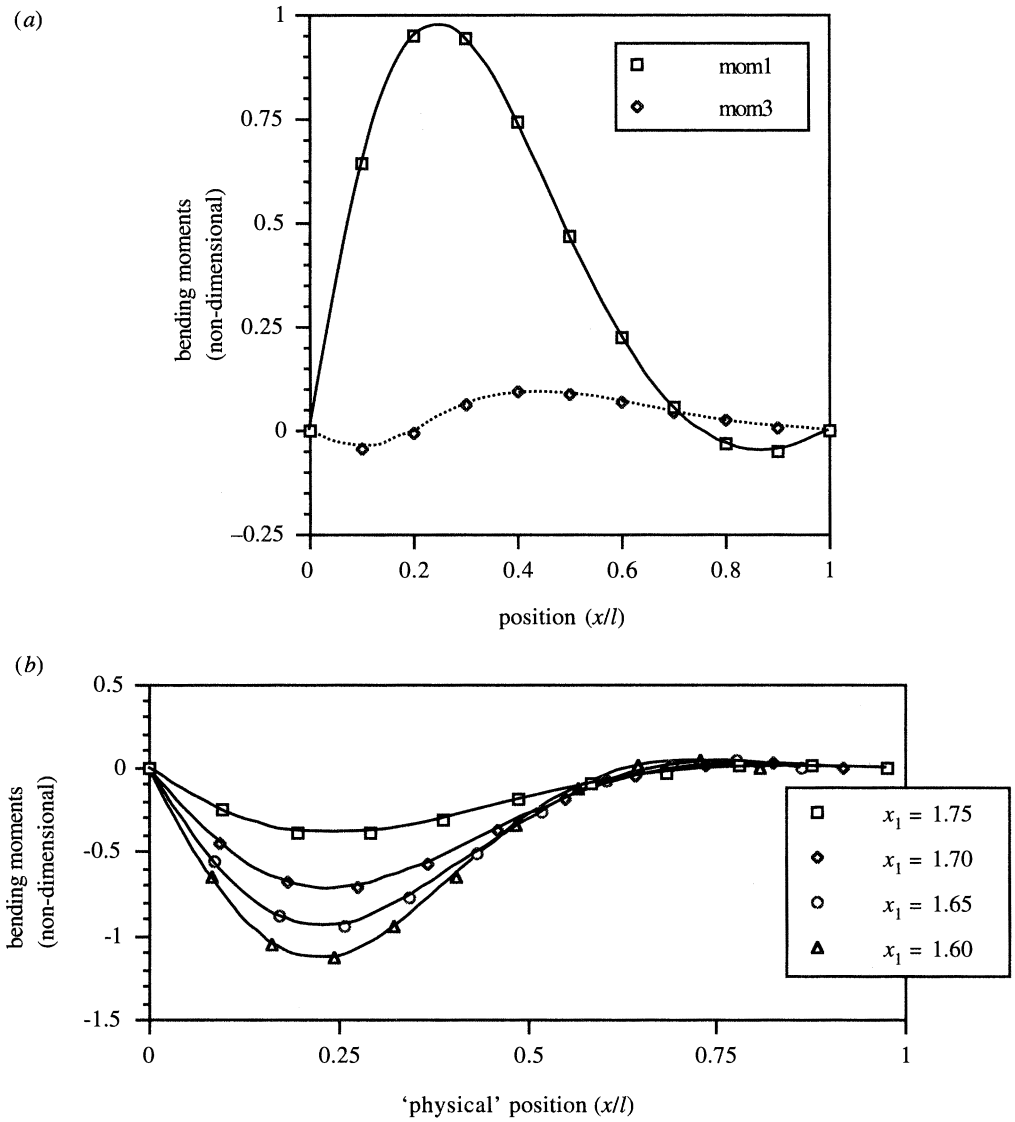

Figure 8. (*a*) Bending moment functions, $l = 4.00$. (*b*) Bending moment, $x_1^{(0)} = 1.77$, $l = 4.00$.

(1) The first-order displacement function is more 'symmetrical' (in relation to the structure's midpoint at $0.5l$) for shorter structural lengths. This is in contrast to the equivalent Euler structural displacement symmetry about its mid-point.

(2) As the top tension x_1 decreases, the top ball joint moves down and the maximum displacement increases quite rapidly. This is accentuated at larger structure lengths: if the top tension is reduced by approximately 10% ($x_1 = 1.60$ and $x_1 = 5.44$ in figures 7*b* and 7*d*, respectively) the maximum displacements are 1.1 and 2.5, respectively.

Figures 8*a–d* plot the first- and second-order bending moments for $l = 4$ and $l = 7.94$. The bending moment—in the same way as the maximum displacement—is larger for $l = 7.94$. Note that the points of maximum bending moments and

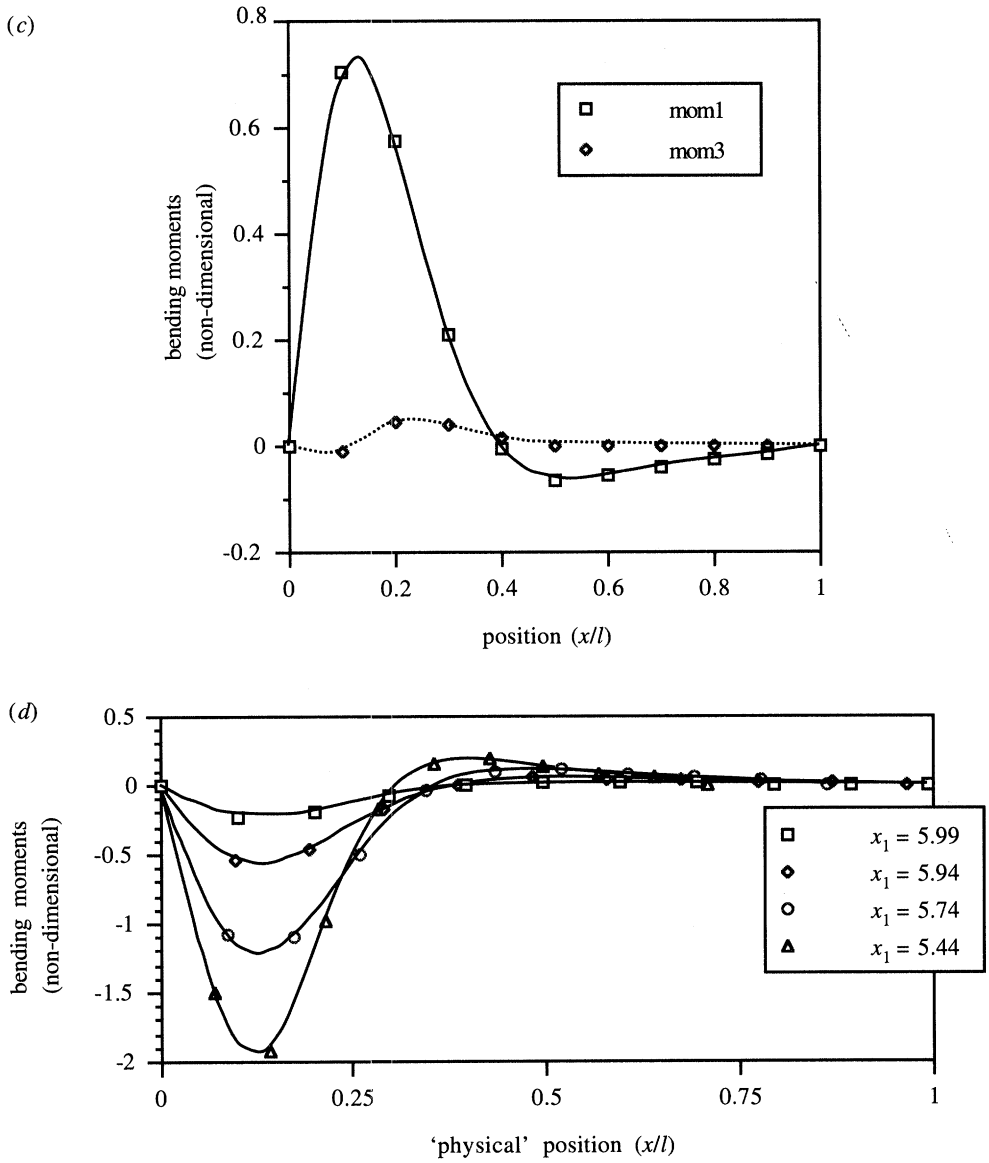

Figure 8. (*c*) Bending moment functions, $l = 7.94$. (*d*) Bending moment, $x_1^{(0)} = 6.00$, $l = 7.94$.

maximum displacements do not coincide. Figure 9*a* and 9*b* present the top tension x_1 in terms of the maximum displacement ζ and the top ball joint vertical displacement δ (positive downwards). It is seen that in both cases a small reduction of the top tension induces a rapid increase in maximum lateral displacement and of the top joint vertical displacement.

The non-dimensionalized parameter variations described above are supplemented by results for specific practical slender structure cases. Table 2 gives data for six representative cases, labelled here as cases A to F. Cases B and F are data typical of a conventional drill pipe and drilling riser, respectively, whereas cases A, C, D and E correspond to nominal data for the Jolliet, Snorre, Hutton and Heidrun tethers,

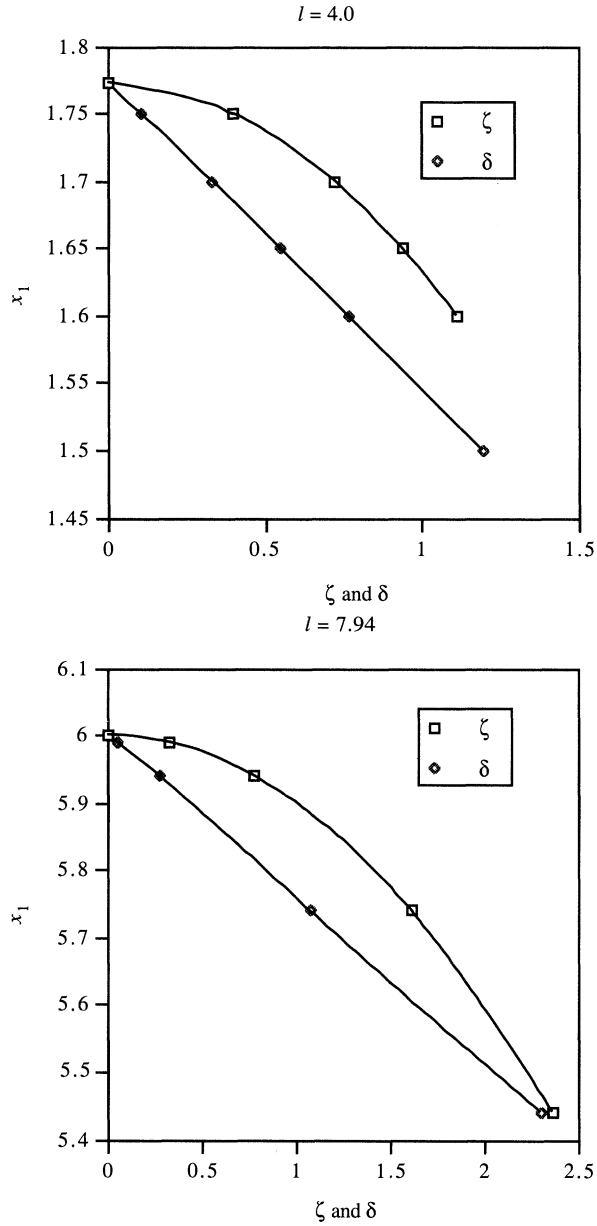

Figure 9. Top tension versus lateral and vertical dispacements: (*a*) $l = 4.0$; (*b*) $l = 7.94$.

respectively—table 1 gives further detailed data on the principal particulars for these platforms. Note that for cases A–F used for illustration here, the parameter p is the submerged weight per unit length, assuming that both the outer fluid and contents of each tubular slender structure are sea water at a density of 1025 kg m^{-3}.

It is clear that the response of these slender structures will be governed by some non-dimensional parameters; table 1 presents some of these. One possible non-dimensional parameter is the position of the neutral point expressed as a fraction of the length of the structure—the parameter l. However, another is the parameter α,

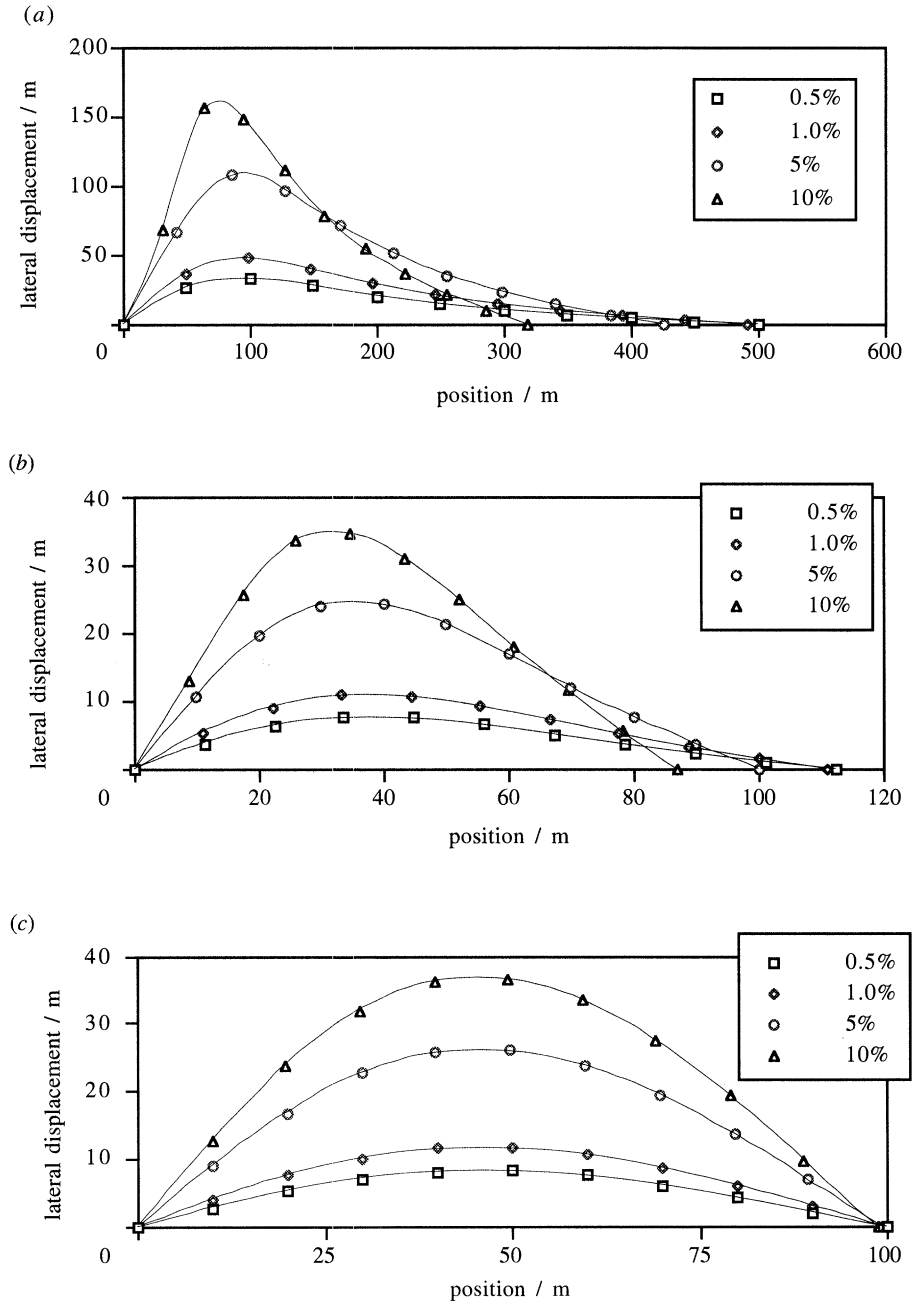

Figure 10. Lateral displacement for reducing top tension: (*a*) case A; (*b*) case D; (*c*) case F.

expressed as

$$\alpha = L\sqrt{\frac{T_{\mathrm{sw}}}{EI}},$$

where L is the structure length, EI is its flexural rigidity and T_{sw} is a characteristic tension taken here to be equal to the self-weight of the structure. A parameter like

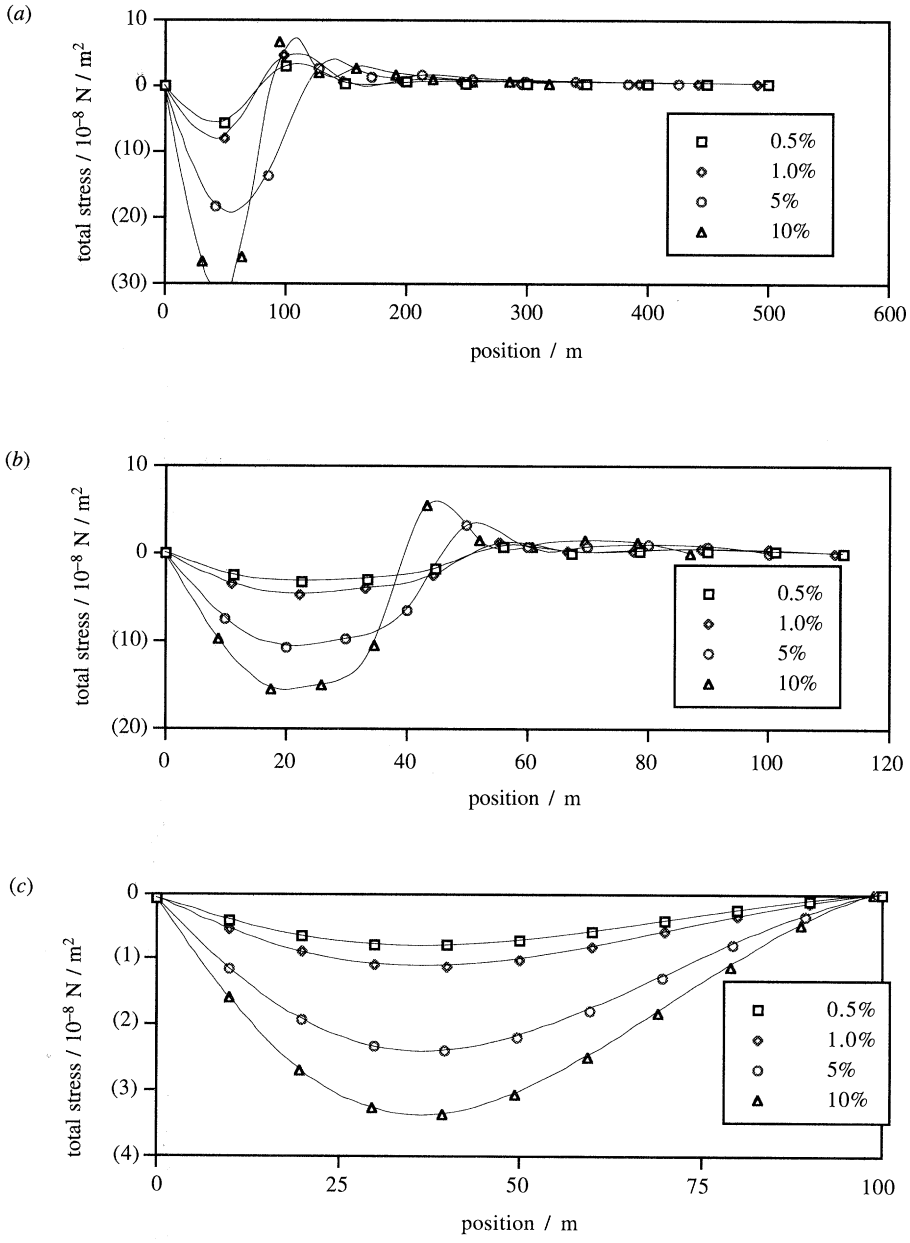

Figure 11. Total stress for reducing top tension: (*a*) case A; (*b*) case D; (*c*) case F.

α arises in the analysis of the bending of bars under constant tension, and, in the cases with variable tension, it is expected that α will still be a useful governing parameter. Therefore, structures listed in table 1 (and the results in figures 2 and 3) are presented in order of decreasing α.

The results for cases A, D and F are presented here as lateral deflection and total (axial plus bending) stress distribution along the structure for reducing values of top tension applied at the upper end. Figures 10*a–c* present the lateral displacements for each of the three cases as the top tension is reduced by values corresponding to 0.5%,

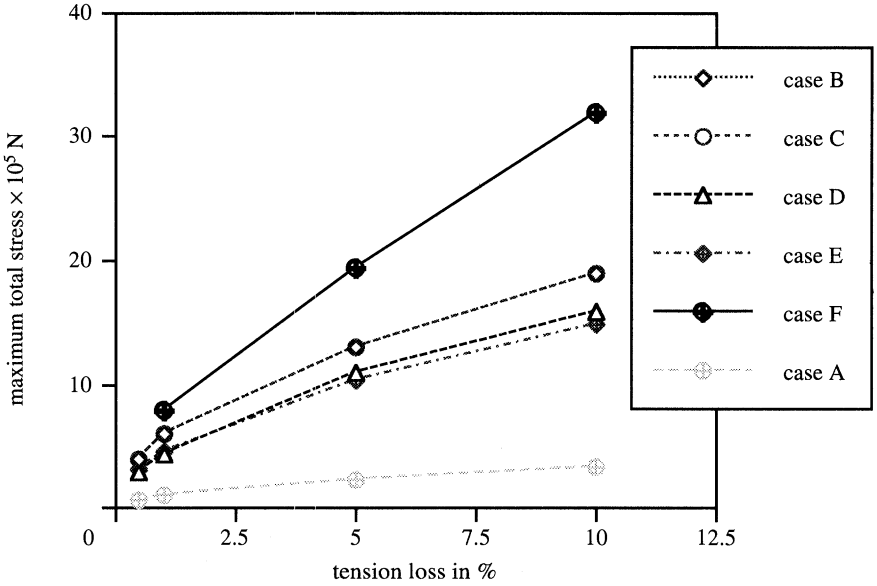

Figure 12. Maximum total stress against tension loss.

Table 2. *Data for case studies*
(Young's modulus for steel is 207 GN m^{-2}. Steel density is 7860 kg m^{-3}.)

parameter	A	B	C	D	E	F
outside diameter/m	0.600	0.127	0.810	0.260	1.118	0.400
inside diameter/m	0.560	0.112	0.734	0.075	1.046	0.370
length/m	513	150	265	114	275	100
$EI/10^6$ N m^2	317.6	1.044	1424.7	46.11	3711.0	69.69
dry mass/kg m^{-1}	286.4	22.13	724.4	382.6	961.8	142.6
p/N m^{-1}	2443.5	188.79	6179.6	3263.7	8205.2	1216.5
m/m	50.66	17.68	61.32	24.17	76.76	38.55
x_1	8.1508	6.0005	2.8923	2.6848	1.1868	−0.1179
ℓ	10.13	8.48	4.32	4.72	3.58	2.59
$T_{crt}/10^6$ N	1.0090	0.020 03	1.0960	0.21179	0.747 48	−0.005 556
$T_{sw}/10^6$ N	1.442	0.0325	1.8832	0.4279	2.595	0.1399
$\alpha = L\sqrt{T_{sw}/EI}$	34.57	26.49	9.635	10.98	7.272	4.480

1.0%, 5% and 10% of its original value. The original value here is taken as the critical top tension at which the slender structure will just begin to buckle. These values are listed in table 2 as T_{crt}. Figures 10–12 present the slender structure response to reductions in top tension below this critical value. Note the comparison between the values of T_{crt} and the tether self-weight T_{sw} in table 2. It is also instructive to note from table 1 that the top tension to tether self-weight ratios for typical TBP structures range from 2.77 to 21.3, whereas here the T_{crt} values being considered are already considerably less. This reduction in top tension leads to a vertical displacement

PHILOSOPHICAL TRANSACTIONS OF THE ROYAL SOCIETY A MATHEMATICAL, PHYSICAL & ENGINEERING SCIENCES

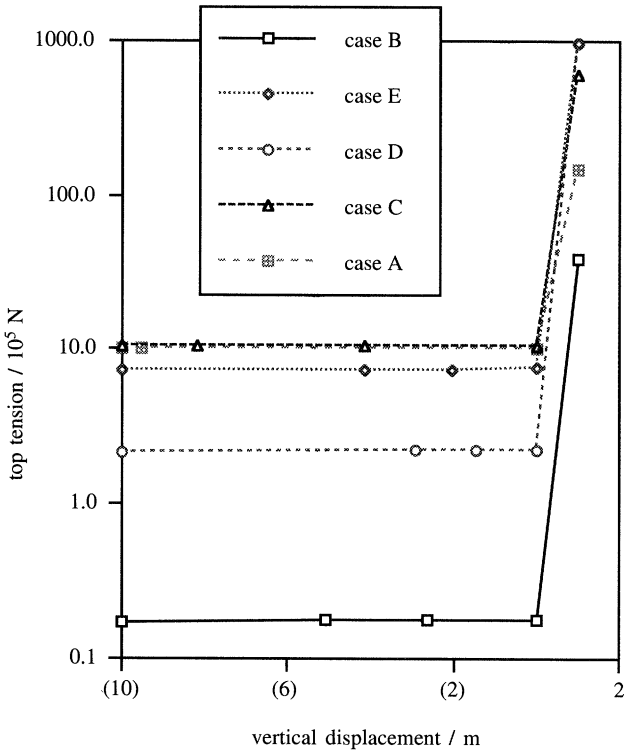

Figure 13. Top tension versus vertical displacement (positive upwards).

of the slender structure upper end towards its lower end. In virtually all the cases presented, the tension reduction of 5% and 10% leads to total stresses which are very large and beyond failure. However, these results have been retained to illustrate the variations that arise. In the same spirit, the very large lateral displacements of the drill pipe (figure 10) are retained despite the fact that they are physically restrained, in practice, by a drill hole. The change of displacement shapes from figure 10*c* for case A with α of 34.02 through to figure 10*a* for case F with α of -4.45 shows the shift from a tension-dominated structure to a stiffness-dominated structure. This is also illustrated in corresponding figures 11*a–c* for the total (axial plus bending) stress distribution in the structures. Note that the numbers in brackets in figures 11–20 are negative values.

For case A, where tension is relatively more important compared to flexural rigidity, the tether buckle is locally large at its lower end with little displacement and stress at the upper two thirds of the tether. As the value of α reduces, this feature gradually reduces and the buckling and stress are distributed more 'uniformly' over the structure length until the marine riser (case F), where the flexural rigidity is relatively more important compared to tension and limits both the lateral displacements and total stress.

It needs to be emphasized that, with the magnitudes of the total stresses shown in figures 11*a–c*, the kind of top tension reductions used here are not feasible. However, the variations seen across these structures point to the fact that a range of α values may, in fact, offer feasible alternative designs. This can be illustrated further by using the maximum total stress calculation to derive a variation of maximum total

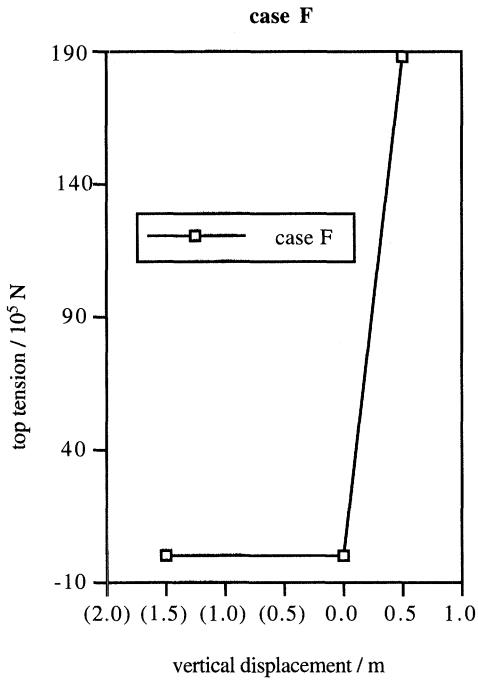

Figure 14. Top tension versus vertical displacement (negative downwards).

stress in the structure against tension loss. Figure 12 illustrates such a curve and shows the change with tension loss for the different structures and their α values. It can be seen that low α values, where the top tension is small compared to flexural rigidity, offer the possibility of vertical structures which can withstand wave-induced vertical movement of the surface platform. Such structures would, of course, continue to provide the horizontal station keeping performance that is the biggest advantage of TBP structures.

Figures 13 and 14 show typical variations of top tension against vertical displacement that are exhibited by the drill pipe and tethers (figure 13) and by the marine riser (figure 14). The step change in the curve between tension and compression in figures 13 and 14 indicates the possibility of severe dynamic instability and snap re-tensioning loads.

Turning now to the results for the forced lateral excitation analysis, cases A, C and E are used to investigate the influence of tether top tension and the amplitude and frequency of upper end excitation on the lateral response.

Figures 15*a*, *b* present lateral deflection and bending stress amplitudes for the case-E structure when its top tension is reduced by 50%. The frequency of excitation and the amplitude of the upper ball joint displacement are taken to be 20 s period 0.31416 rad s^{-1} and 0.3 m, respectively. Note that although figure 15 does not show phase information, figure 18, described subsequently, presents response phase angle results which lead to a 'negative' restoring force (which is in phase with the platform displacement), thus causing the slender structure's force on the platform to accentuate (rather than restore) its motion.

The frequency of excitation of the upper end of the structure plays an important role in its lateral dynamics, especially at reduced top tensions. Figures 16*a*, *b* present results for the case-A structure with its upper end vibrated at an amplitude of 0.3 m

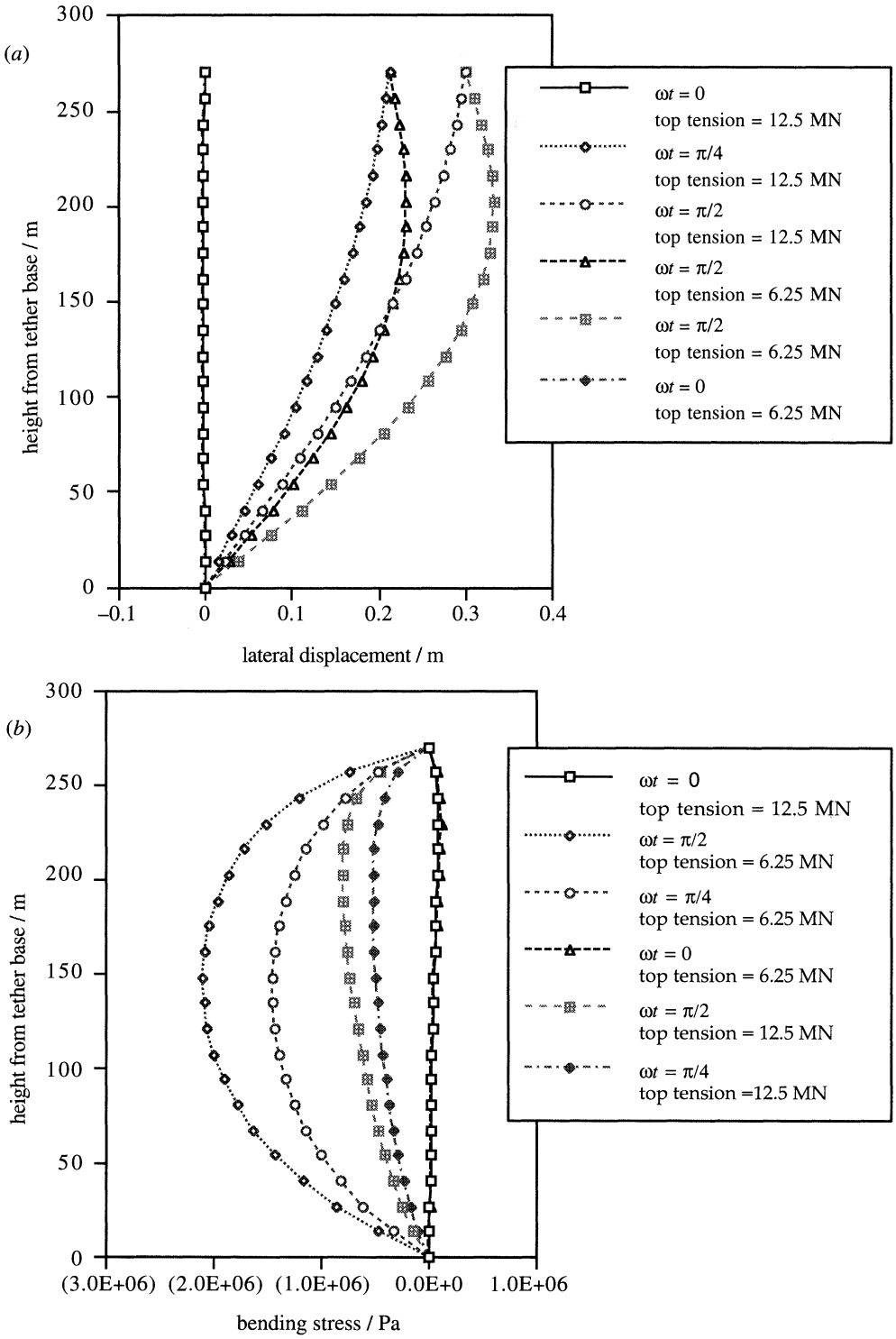

Figure 15. Case E: (*a*) lateral displacement; (*b*) bending stress.

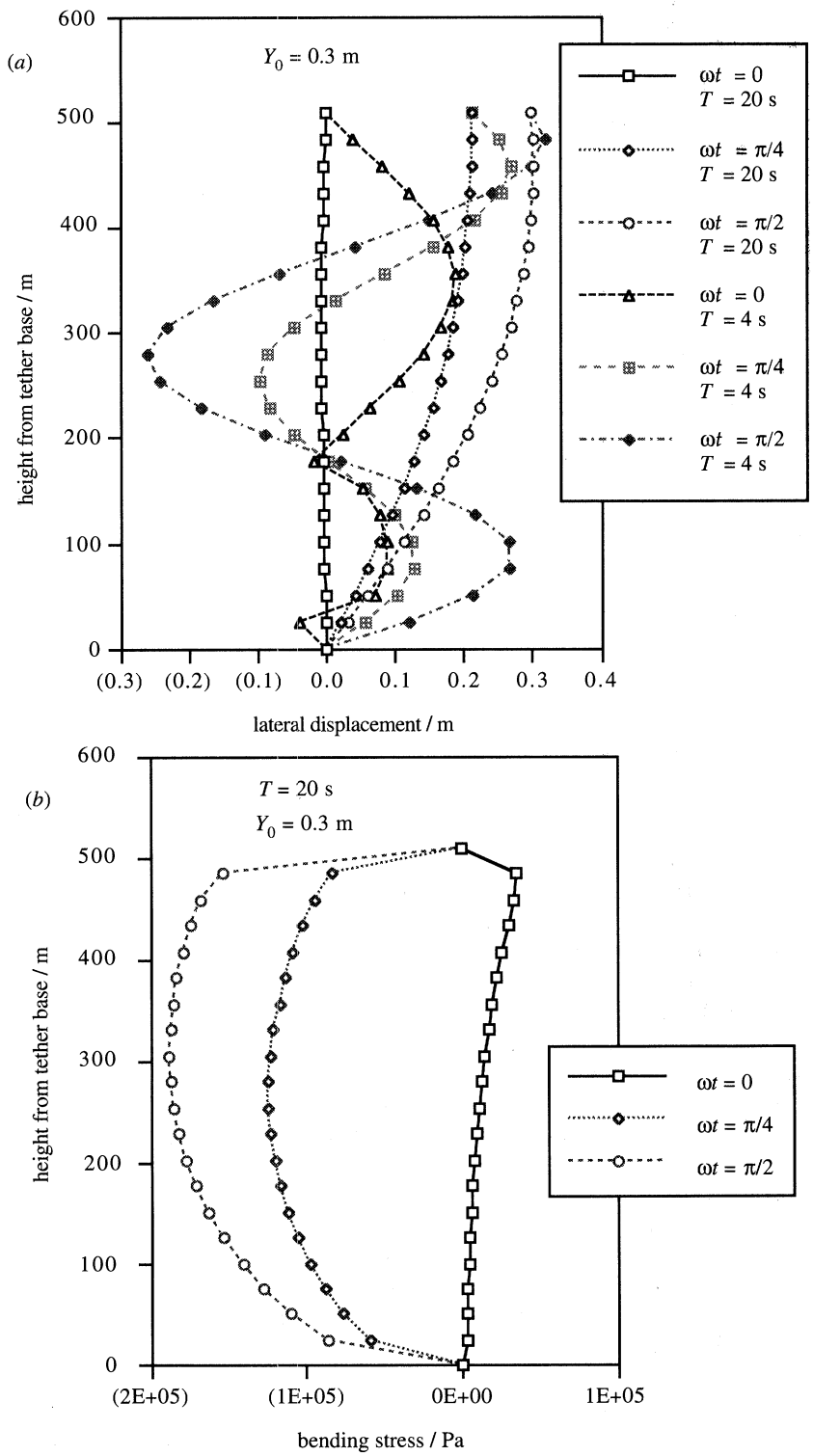

Figure 16. Case A: (*a*) lateral displacement; (*b*), (*c*), bending stresses.

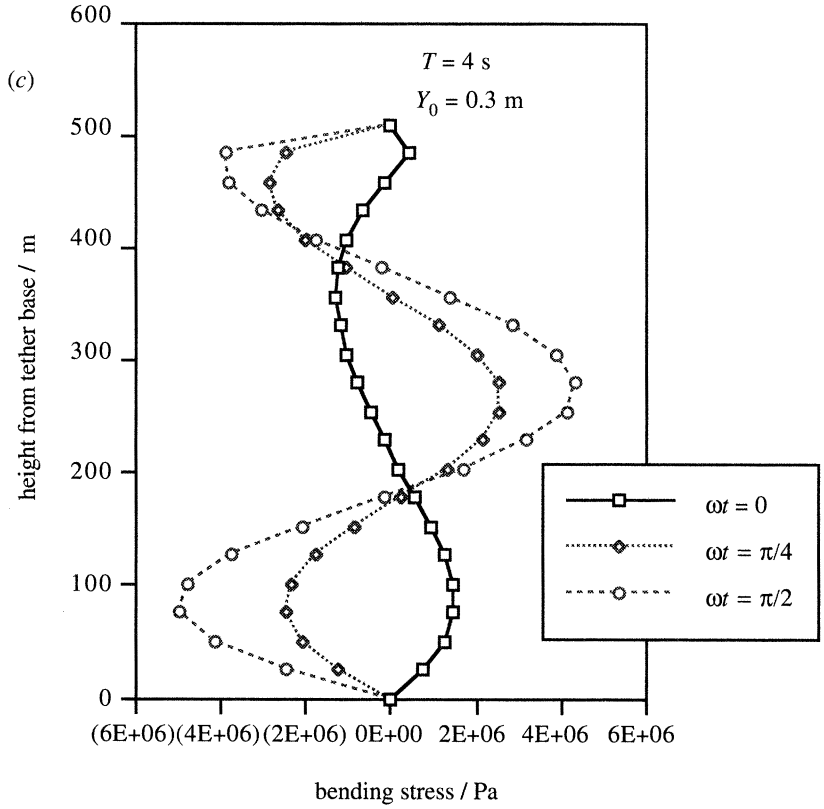

Figure 16. Cont.

and two periods of excitation of 4 and 20 s for a top tension of 1.85 MN. When the forced excitation occurs at 20 s period, the total tether lateral displacement is basically dominated by the rigid-body motion and, hence, bending stresses are relatively low. On the other hand, for 4 s period, the elastic modes are significantly excited and lateral displacements and bending stresses become significant.

The linearized damping term is dependent on y_0 (through $\bar{b}_l$) so results are expected to vary with the amplitude of the upper ball joint displacement. This dependence may be more critical near a resonance frequency and virtually imperceptible outside this area. Figures 17*a*, *b* show results for the case-C structure for two periods of excitation, of 4 and 20 s, and for two amplitudes of upper ball joint displacement, of 0.5 and 1.5 m. The top tension is taken to be 9.0 MN.

From Figure 17*a*, it can be observed that the normalized lateral displacements at 20 s period are nearly linear, but for the 4 s period this normalized displacement is quite dependent on y_0. Note that the restoring forces for 20 s period are nearly in phase with tether top end displacement, but this does not hold true at 4 s period.

Figures 18–20 show the effect of reducing tension on the amplitude and phase of the horizontal restoring force applied by the structures on the surface platform for cases A, C and E, respectively. These figures clearly demonstrate the variations of amplitude and phase that produce the accentuating rather than restoring force at some frequencies mentioned earlier. The changes in natural frequencies due to reduction in top tension are also clearly evident.

However, as explained subsequently, because the tether restoring forces have a rela-

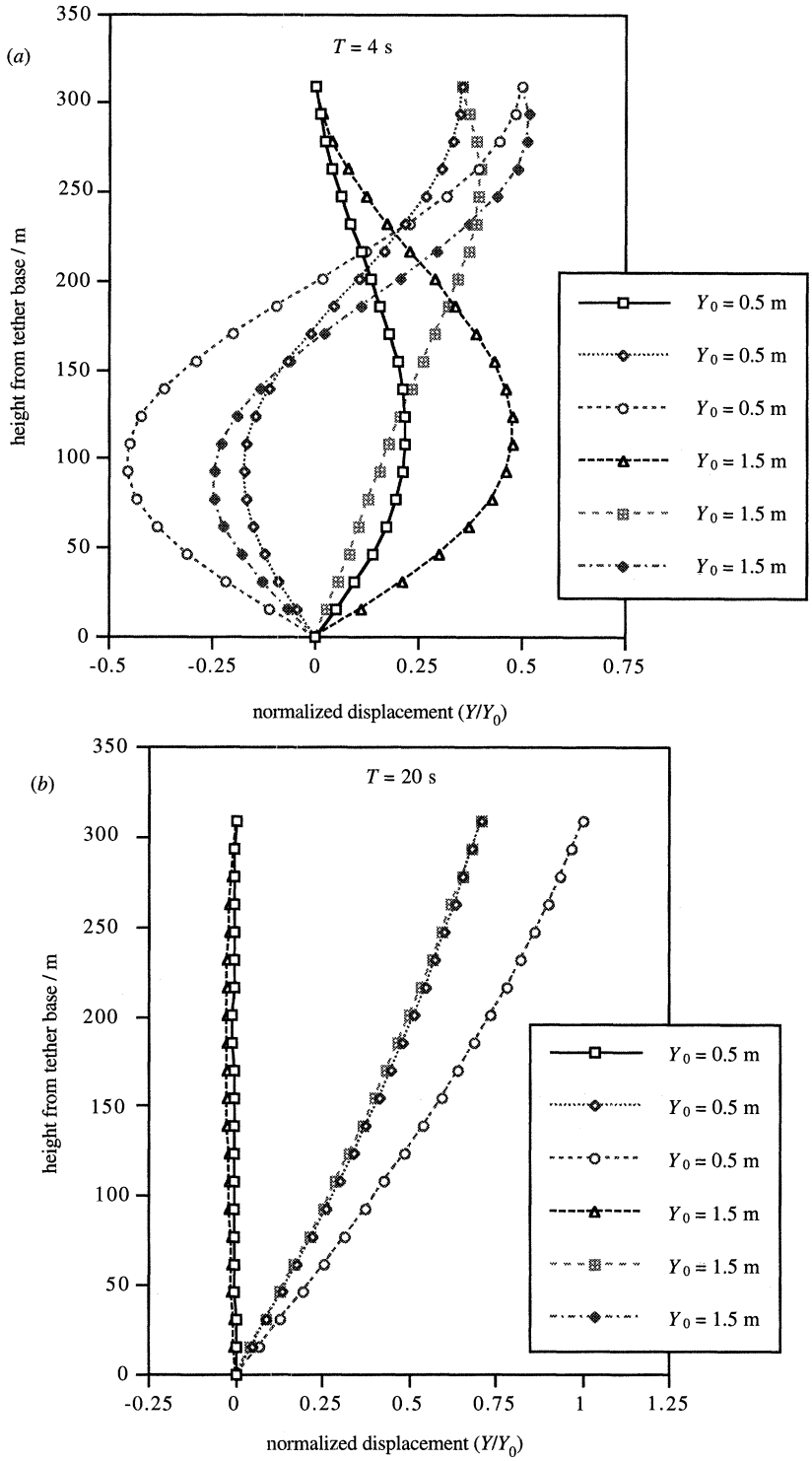

Figure 17. Case C: (*a*) normalized displacement (Y/Y_0); (*b*) lateral displacement; (*c*), (*d*) bending stress.

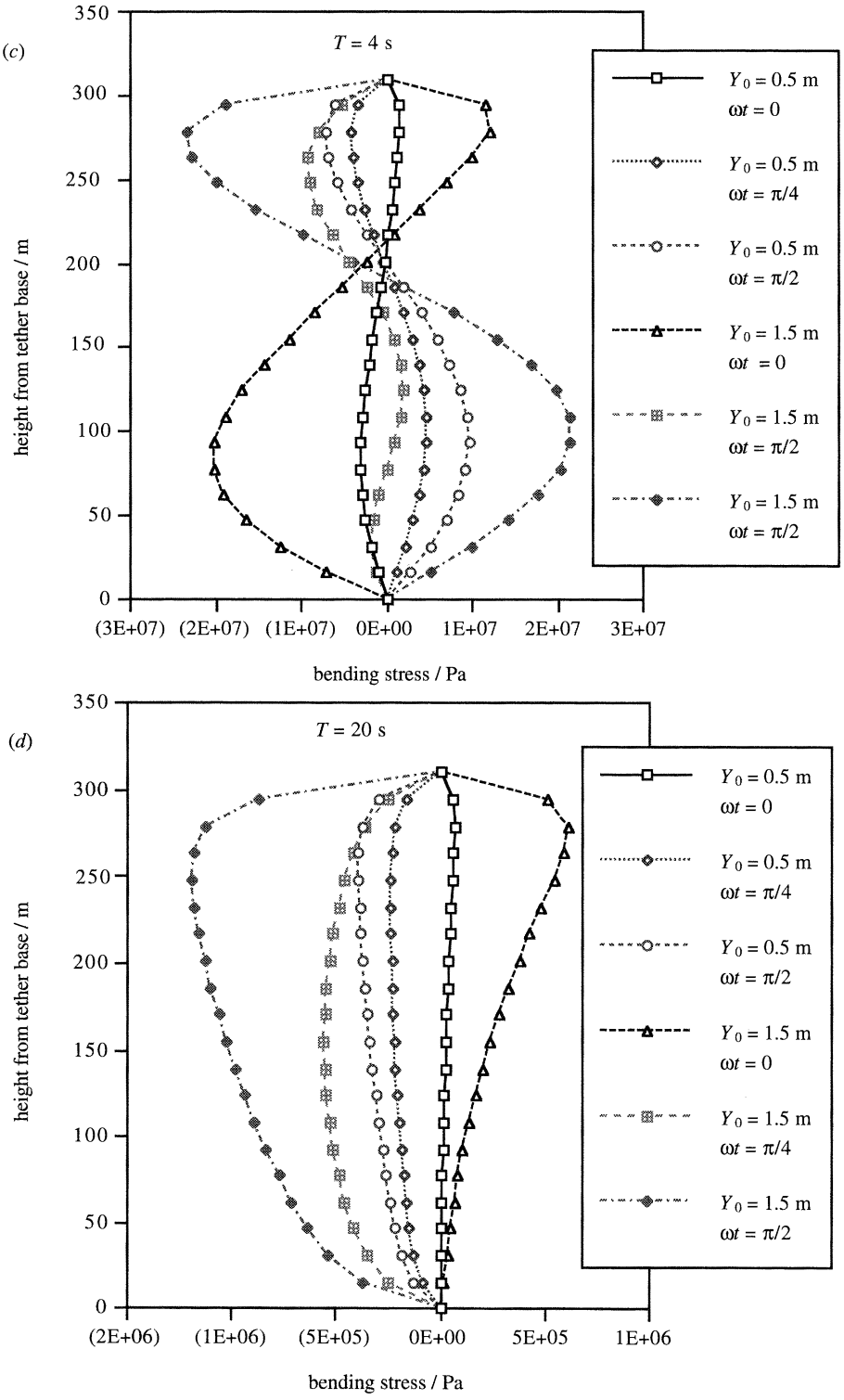

Figure 17. Cont.

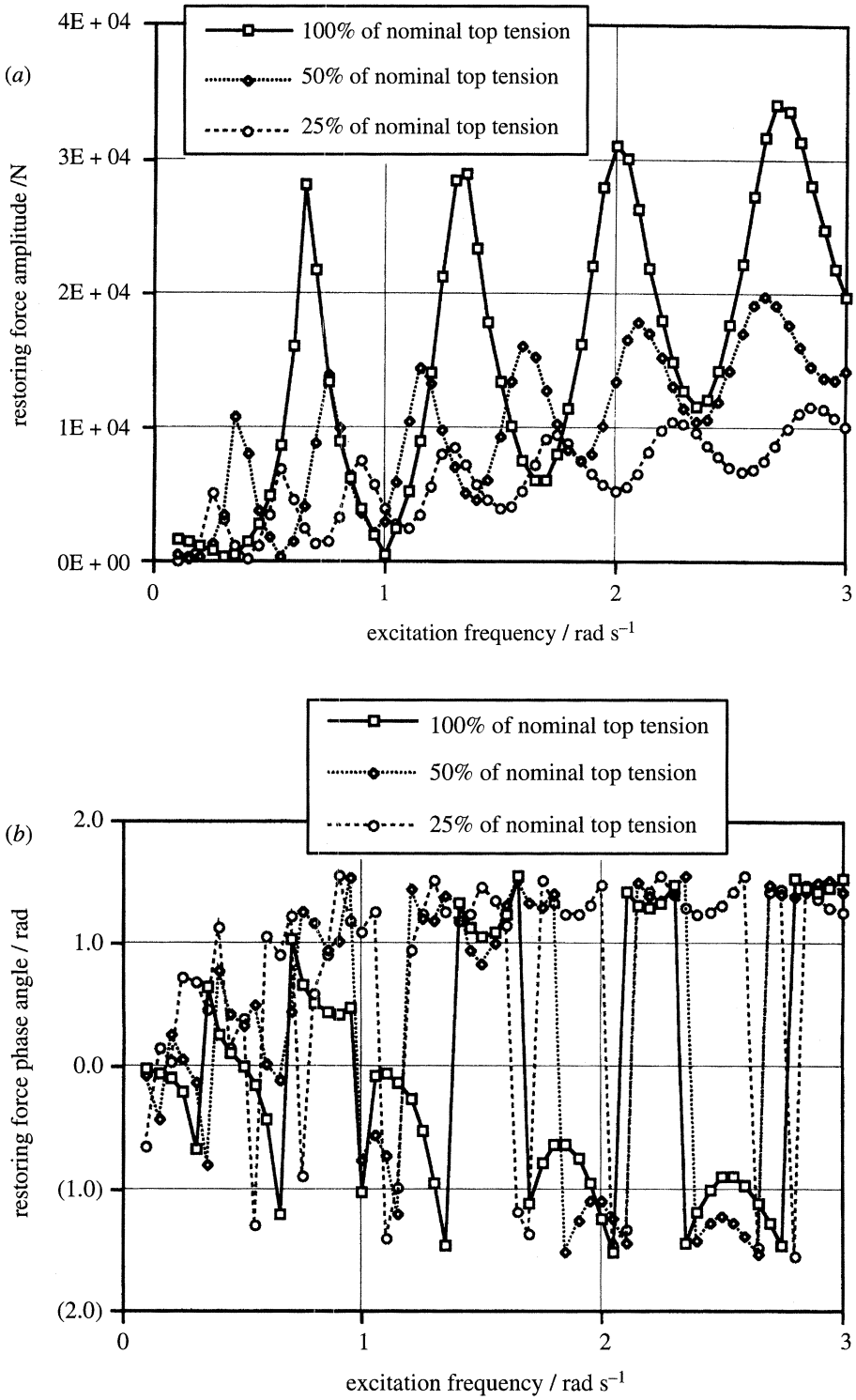

Figure 18. Case A. Restoring force amplitude and phase response as a function of top tension.

PHILOSOPHICAL TRANSACTIONS OF THE ROYAL SOCIETY A MATHEMATICAL, PHYSICAL & ENGINEERING SCIENCES

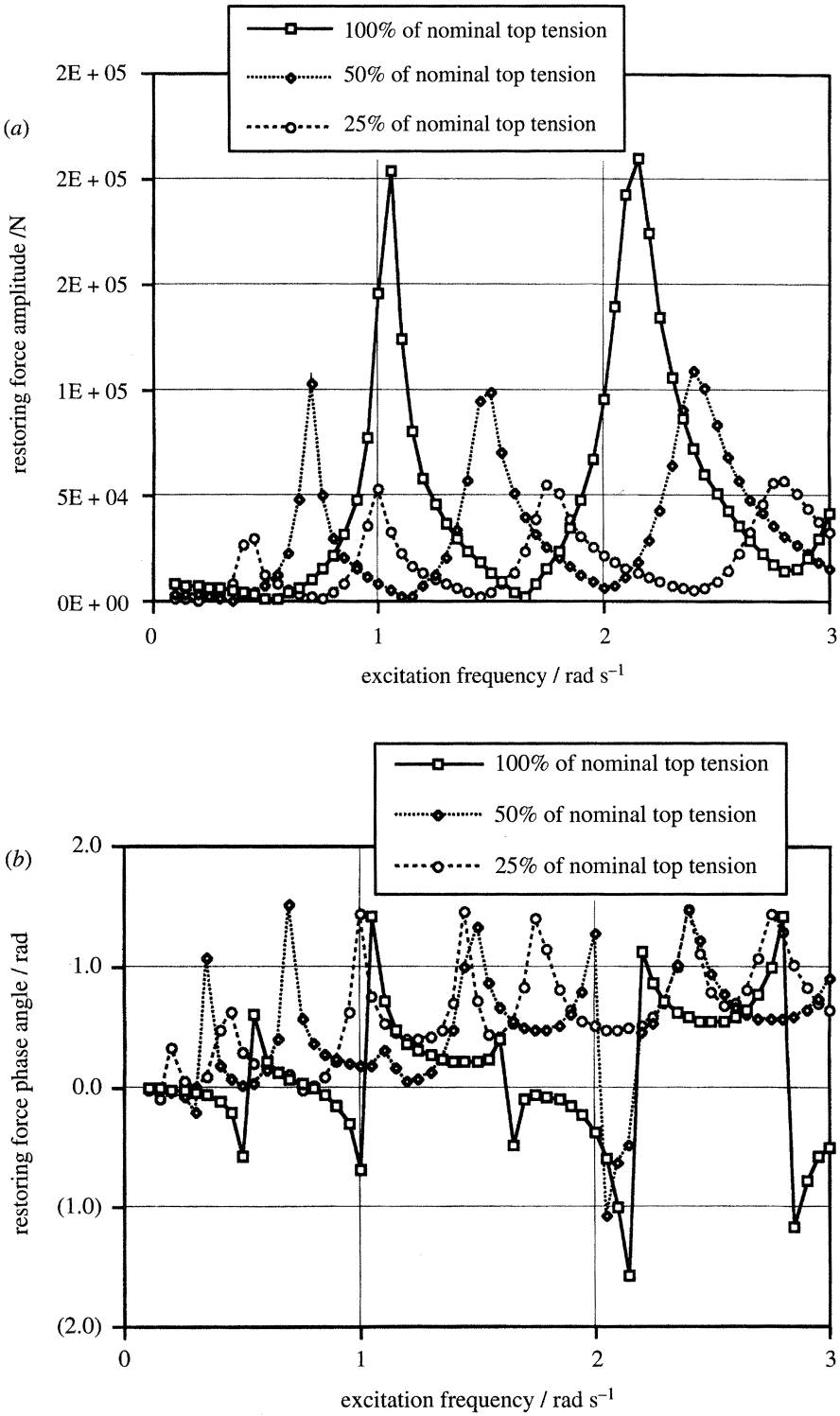

Figure 19. Case C. Restoring force amplitude and phase response as a function of top tension.

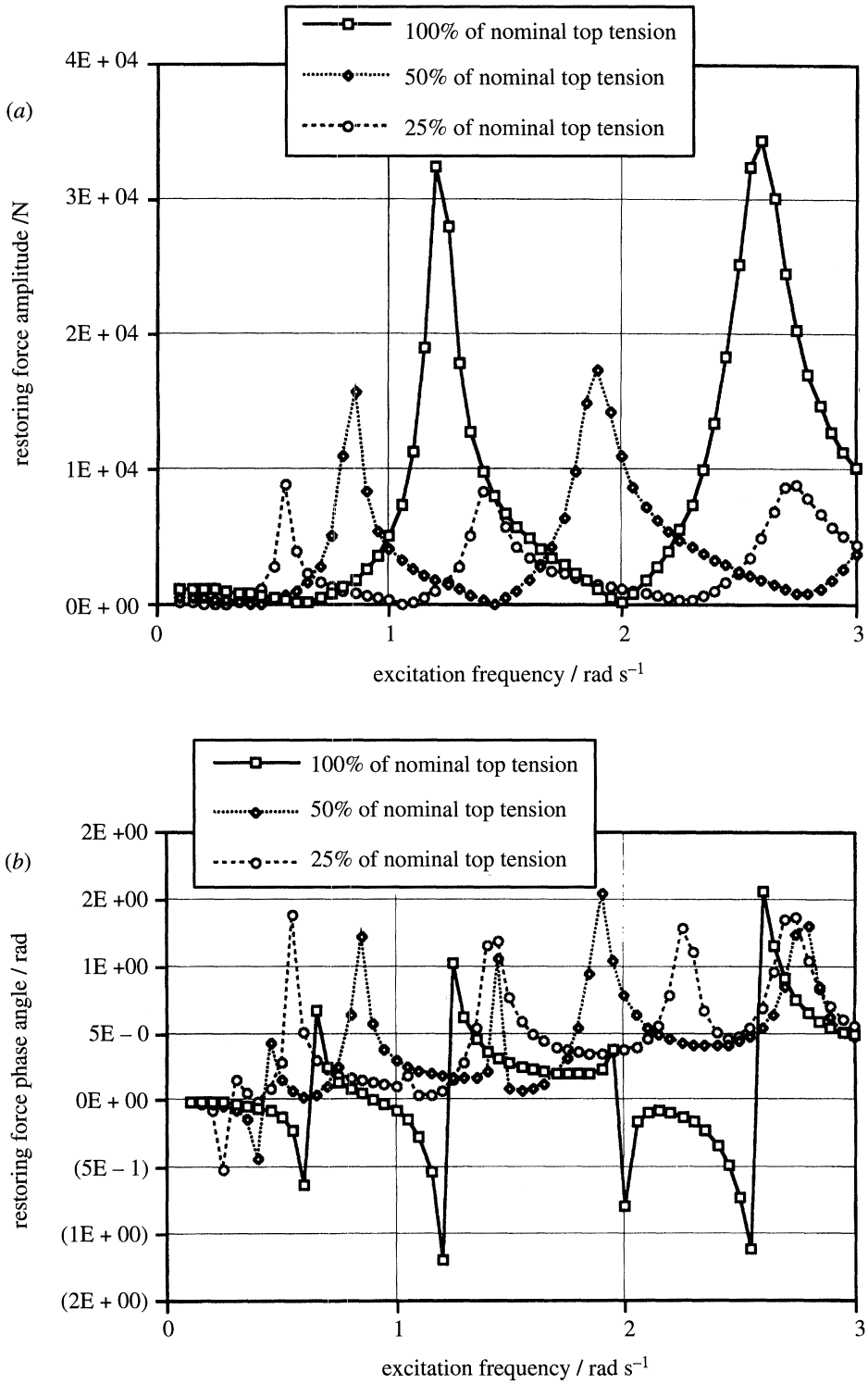

Figure 20. Case E. Restoring force amplitude and phase response as a function of top tension.

tively small effect on surface platform motion, which are inertia, rather than stiffness dominated, they will have a small effect on global platform response. This is, however, being investigated further by examining combined platform–tether responses in subsequent work.

5. Conclusions

The theory and illustrative results presented in this paper demonstrate the applicability of a second-order buckling theory, which can be used to evaluate the behaviour of slender marine structures at low tension. The theory takes the variation of tension with length along the structure into account as well as second-order effects brought into play by large deflections.

The case-study results suggest that the design of structural cross sections at low tension will need to move towards more stiffness-dominated structures capable of withstanding larger vertical movements of their upper end through both tension and compression phases. On the other hand, the forced vibration calculations presented here show that the slender structures considered are surprisingly tolerant of this forcing at reduced tension, although, in general terms, both the lateral deflection and bending stresses do increase. An interesting feature of the structure's lateral response force on the surface platform is that depending on the frequency of oscillation, this restoring force is either in-phase or out-of-phase with displacement to yield a force that accentuates motions. This phenomenon occurs also with tethers at conventional mean tensions but does so at rather higher frequencies than would be encountered within the wave range (see Jefferys & Patel 1982). However, since dynamic restoring forces from the tether have a negligible influence on surface platform motions, this behaviour is not significant.

Another interesting element of the analysis is an estimation of the likely errors introduced by using the equivalent energy-based linearization operating on 'rocking' rigid-body motion of the tether. This feature has also been examined previously by Jefferys & Patel (1982) and Patel & Lynch (1983) for tethers at conventional tensions, with results showing that the effects of this assumption are relatively small except in a narrow region around the first-tether resonant frequency. At reduced tension, of course, these frequencies may lie closer to wave frequencies.

The work reported here has demonstrated that the lateral dynamics of tethers at reduced mean tension is unlikely to pose a design problem in itself. The reduced mean tension will lead to increased natural periods in surge, sway and yaw, but would leave the natural periods in heave, roll and pitch unchanged for small amplitudes of motion. The real design problem arises when a platform with reduced mean tether tension is subjected to vertical platform motion sufficiently large so as to take the tether into compression followed by the dynamic stresses induced by the tether going back into tension. Work elsewhere (Patel & Park 1992) indicates that, under certain conditions of tether EI value and compression–tension cycling, the tether can behave satisfactorily.

This work was carried out with the support of the facilities of the Santa Fe Laboratory for Offshore Engineering (University College London) and the Laboratory for Submarine Technology (Federal University of Rio de Janeiro). M.A.V. acknowledges the support of the Brazilian Council of Research (CNPq) for this work. The authors would also like to express their gratitude to Mr Thomas Wilne for his assistance in the preparation of this paper.

Appendix A. Curvature and end shortening

El Naschie (1990) presents detailed information on how curvature and end shortening are derived. He considers a strut defined by lateral deflection, ω, as a function of longitudinal distance, x. The original length, l, of the strut is reduced by distance, δ, and its curvature κ is defined as the rate of change of angle ψ with length. Then,

$$\kappa = \mathrm{d}\psi/\mathrm{d}s, \tag{A 1}$$

where s is distance along the strut, and

$$\psi = \sin^{-1}(\mathrm{d}w/\mathrm{d}s). \tag{A 2}$$

Hence, substituting equation (A 2) into (A 1) and taking into account that $\mathrm{d}x = \mathrm{d}s$ (as it is assumed that the strut is inextensible) results in

$$\kappa = \frac{w''}{\sqrt{1-w'^2}}. \tag{A 3}$$

The vertical displacement of the upper ball joint, δ, is calculated next. For an infinitesimal element of the strut

$$(\mathrm{d}s)^2 = (\mathrm{d}x - \mathrm{d}u)^2 + (\mathrm{d}w)^2, \tag{A 4}$$

where $\mathrm{d}s$ is distance along the curved strut, $\mathrm{d}x$ is distance along its original straight length, $\mathrm{d}u$ is the axial foreshortening of the strut due to its curvaure and $\mathrm{d}w$ is the change in lateral deflection over the distance $(\mathrm{d}x-\mathrm{d}u)$. Hence, dividing equation (A 4) by $\mathrm{d}x$ $(= \mathrm{d}s)$, rearranging and then integrating from $x = 0$ to $x = l$ results in

$$\delta = \int_0^l \left(1 - \sqrt{1-w'^2}\right) \mathrm{d}x. \tag{A 5}$$

Substituting equation (2.4 *c*) in (A 5), and assuming small inclinations result in

$$\delta = \int_0^l \left[\frac{1}{2}\left(\sum_{n=1}^{3N} D_n \cos\left(\frac{n\pi}{l}x\right)\right)^2\right] \mathrm{d}x, \tag{A 6}$$

where

$$D_n = (n\pi/l)[\zeta a_n + \zeta^3 \bar{b}_n], \quad \text{if } 1 \leqslant n \leqslant N,$$
$$D_n = (n\pi/l)\zeta^3 d_n, \quad \text{if } N+1 \leqslant n \leqslant 3N,$$

and finally, integrating equation (A 6) produces

$$\delta = \tfrac{1}{4} l \sum_{n=1}^{3N} D_n^2. \tag{A 7}$$

Appendix B. Calculating the point of maximum displacement

Equation (2.8 *a*) can be rewritten as

$$a_1 \cos\tilde{\theta} + 2a_2 \cos 2\tilde{\theta} + \cdots + (N-1)a_{(N-1)} \cos(N-1)\tilde{\theta} + N a_N \cos N\tilde{\theta} = 0, \tag{B 1}$$

where $\tilde{\theta} = \pi\tilde{x}/l$. Equation (B 1) can be rewritten by using $\cos n\tilde{\theta} = \frac{1}{2}(\mathrm{e}^{\mathrm{i}n\tilde{\theta}} + \mathrm{e}^{-\mathrm{i}n\tilde{\theta}})$ and $\mathrm{e}^{\mathrm{i}n\tilde{\theta}} = y^n$. Then,

$$a_1(y+y^{-1}) + 2a_2(y^2+y^{-2}) + \cdots + (N-1)a_{(N-1)}(y^{(N-1)}+y^{-(N-1)}) + N a_N(y^N+y^{-N}) = 0, \tag{B 2 *a*}$$

or

$$Na_N y^{2N} + (N-1)a_{(N-1)}y^{(2N-1)} + \cdots + a_1 y^{(N+1)} + 0y^N + a_1 y^{(N-1)} + \cdots + (N-1)a_{(N-1)}y + Na_N = 0. \quad (B\,2\,b)$$

Finally, the roots of the polynomial equation (B 2 *b*) may be calculated.

Appendix C. Deriving the second-order governing equation

The right-hand side of equation (2.9 *a*) can be simplified to yield

$$\sum_{i=1}^{N}\sum_{j=1}^{N}\sum_{k=1}^{N} \sin(j\pi x/l)[A_{ijk}\cos(i\pi x/l)\cos(k\pi x/l) + \sin(i\pi x/l)\sin(k\pi x/l)] + x_2^{(2)}\sum_{i=1}^{N}\bar{a}_i \sin(i\pi x/l), \quad (C\,1)$$

where

$$A_{ijk} = -a_i a_j a_k(\pi/l)^6 ij^2 k[\tfrac{1}{2}j^2 + 3k^2], \quad B_{ijk} = a_i a_j a_k(\pi/l)^6 i^2 j^2 k^2, \quad \bar{a}_i = a_i(\pi/l)^2 i^2.$$

Equation (C 1) can be sequentially simplified using product-to-sum trigonometric identities to produce equation (C 3). Hence,

$$\sum_{i=1}^{N}\sum_{j=1}^{N}\sum_{k=1}^{N} \tfrac{1}{2}A_{ijk}[\cos((i+k)\pi x/l) + \cos((i-k)\pi x/l)]\sin(j\pi x/l) + \sum_{i=1}^{N}\sum_{j=1}^{N}\sum_{k=1}^{N} \tfrac{1}{2}B_{ijk}[\cos((i-j)\pi x/l) - \cos((i+j)\pi x/l)]\sin(k\pi x/l) + x_2^{(2)}\sum_{i=1}^{N}\bar{a}_i \sin(i\pi x/l), \quad (C\,2)$$

or

$$\sum_{i=1}^{N}\sum_{j=1}^{N}\sum_{k=1}^{N} [AA_{ijk}[\sin((i+j+k)\pi x/l) - \sin((i-j+k)\pi x/l)] + BB_{ijk}[\sin((i+j-k)\pi x/l) - \sin((i-j-k)\pi x/l)]] + x_2^{(2)}\sum_{i=1}^{N}\bar{a}_i \sin(i\pi x/l), \quad (C\,3)$$

where $AA_{ijk} = \frac{1}{4}(A_{ijk} - B_{ijk})$ and $BB_{ijk} = \frac{1}{4}(A_{ijk} + B_{ijk})$. Finally, equation (2.6 *b*) may be rewritten as

$$w_3'''' + (x_2^{(0)} - x)w_3'' - w_3' = \sum_{i=1}^{N}[C_i + x_2^{(2)}\bar{a}_i]\sin(i\pi x/l) + \sum_{i=N+1}^{3N} C_i \sin(1\pi x/l), \quad (C\,4)$$

where the coefficients C_i are linear combinations of AA_{ijk} and BB_{ijk} from equation (C 3).

Appendix D. Calculating bending moment and stress

The non-dimensional bending moment $\bar{m}(x)$ is given by

$$\bar{m}(x) = \zeta w_1'' + \zeta^3(w_3'' + \tfrac{1}{2}(w_1'^2 w_1'')) \tag{D 1}$$

or, substituting equations (2.7 *a*) and (2.12) into (D 1) results in

$$\bar{m}(x) = -\Bigg[\zeta \sum_{n=1}^{N} a_n (n\pi/l)^2 \sin(n\theta) + \zeta^3 \sum_{n=1}^{N} \bar{b}_n (n\pi/l)^2 \sin(n\theta) + \zeta^3 \sum_{n=N+1}^{3N} d_n (n\pi/l)^2 \sin(n\theta) + \zeta^3 \sum_{i=1}^{N}\sum_{j=1}^{N}\sum_{k=1}^{N} \bar{A}_{ijk} \cos(i\theta)\cos(j\theta)\cos(k\theta)\Bigg], \tag{D 2 a}$$

where $\theta = \pi x/l$ and $\bar{A}_{ijk} = 0.5 a_i a_j a_k ijk^2 \pi^4/l^4$, or simplifying equation (D 2 *a*) produces

$$\bar{m}(x) = -\Bigg[\zeta \sum_{n=1}^{N} \bar{a}_n \sin(n\theta) + \zeta^3 \sum_{n=1}^{N} \bar{\bar{b}}_n \sin(n\theta) + \zeta^3 \sum_{n=N+1}^{3N} \bar{d}_n \sin(n\theta) + \zeta^3 \sum_{i=1}^{N}\sum_{j=1}^{N}\sum_{k=1}^{N} \bar{A}_{ijk}[\sin(i+j+k)\theta - \sin(i+j-k)\theta + \sin(i-j+k)\theta - \sin(-+j-k)\theta]\Bigg], \tag{D 2 b}$$

where

$$\bar{a}_n = (n\pi/l)^2 a_n, \quad \bar{d}_n = (n\pi/l)^2 d_n, \quad \bar{A}_{ijk} = \tfrac{1}{4}\bar{A}_{ijk}, \quad \bar{\bar{b}}_n = (n\pi/l)^2 \bar{b}_n.$$

Further simplifying equation (D 2 *b*) results in

$$\bar{m}(x) = -\zeta \sum_{n=1}^{N} \bar{a}_n \sin(n\theta) - \zeta^3 \Bigg[\sum_{n=1}^{N} \bar{\bar{b}}_n \sin(n\theta) + \sum_{n=N+1}^{3N} \bar{d}_n \sin(n\theta) + \sum_{i=1}^{3N} \bar{B}_n \sin(n\theta)\Bigg] \tag{D 2 c}$$

and finally, the non-dimensional bending moment is given by

$$\bar{m}(x) = -[\zeta m_1(x) + \zeta^3 m_3(x)], \tag{D 2 d}$$

$$m_1(x) = \sum_{n=1}^{N} \bar{a}_n \sin(n\theta), \tag{D 2 e}$$

$$m_1(x) = \sum_{n=1}^{3N} \bar{\bar{B}}_n \sin(n\theta), \tag{D 2 f}$$

where

$$\bar{\bar{B}}_n = \bar{\bar{b}}_n + \bar{B}_n, \quad \text{if } 1 \leqslant n \leqslant N,$$

$$\bar{\bar{B}}_n = \bar{d}_n + \bar{B}_n, \quad \text{if } n \geqslant N+1.$$

The bending stress $\sigma_B(x)$ is given by

$$\sigma_B(x) = \frac{M(x)}{I}\frac{OD}{2}, \tag{D 3 a}$$

where OD is the pipe outside diameter. But $M(x) = pm^2\bar{m}(x)$, then

$$\sigma_{\mathrm{B}}(x)/E = \tfrac{1}{2}\bar{m}(x)od, \tag{D 3 b}$$

where $od = OD/m$. The total axial stress $\bar{\sigma}(x)$ is given by

$$\bar{\sigma}(x) = |\sigma_{\mathrm{B}}(x)| + |\sigma_{\mathrm{T}}(x)|, \tag{D 4}$$

where $\sigma_{\mathrm{T}} = \frac{1}{16}E(od^2 + id^2)[(x_1 + x_2)x/l - x_2]$ and $id = ID/m$.

Appendix E. Determination of the equivalent linear damping

The energy dissipated, in one cycle, by the linear and nonlinear damping are, respectively,

$$E_{\mathrm{l}} = \int_0^{2\pi l\omega} b_{\mathrm{l}} \left[\frac{\partial y}{\partial t}\right]^2 \mathrm{d}t, \tag{E 1 a}$$

$$E_{\mathrm{nl}} = \int_{-l2\omega}^{2\pi l2\omega} b_{\mathrm{nl}} \left[\frac{\partial y}{\partial t}\right]^3 \mathrm{d}t, \tag{E 1 b}$$

where

$$\frac{\partial y}{\partial t} = \left\{\left[x + \sum_{n=1}^{N} a_n \sin(n\pi x/l)\right]\cos\omega t - \left[\sum_{n=1}^{N} b_n \sin(n\pi x/l)\right]\sin\omega t\right\}\omega\frac{y_0}{l}. \tag{E 1 c}$$

The relationship between b_{l} and b_{nl} can be obtained by substituting equation (E 1 c) in (E 1 a) and (E 1 b) and then making $E_{\mathrm{l}} = E_{\mathrm{nl}}$. However, the result is a very complicated expression for the equivalent damping because it depends on the unknown elastic modes. In this paper the contribution of the elastic will be disregarded for the calculation of the equivalent damping. Hence, the following relationship is found:

$$b_{\mathrm{l}} = \frac{8}{3\pi}\frac{\omega y_0}{l} x b_{\mathrm{nl}}. \tag{E 1 d}$$

References

Addison, G. D. & Steinsvik, B. 1976 Tethered production platform system. *Proc. Offshore North Sea Conf.* (London).

Albrecht, H. G., Koenig, D. & Kokkinowrackos, K. 1978 Nonlinear dynamic analysis of tension leg platforms for medium and greater depth. *Offshore Technology Conf., OTC 3044*, pp. 7–15.

Annon 1975 New platform begins offshore test. *Oil and Gas Jl*, 5th May, 59–60.

Capanoglu, C. 1979 Tension-leg platform design: interaction of naval architectural and structural design considerations. *Marine Technol.* **16**, 343–352.

Davies, K. B., Leverette, S. J. & Spillane, M. W. 1994 Ringing response of TLP and GBS platforms. In *7th Behaviour of Offshore Structures, BOSS'94* (ed. C. Chryssostomidis), vol. 2, pp. 569–585. Oxford: Pergamon.

El Naschie, M. S. 1990 *Stress, stability and chaos in structural engineering: an energy approach.* New York: McGraw-Hill.

Fines, S. 1993 Tensional buoyant platforms—now and in the future. In *Proc. of Seminar on Tensional Buoyant Platforms—Analysis, Design and Field Experience* (ed. M. H. Patel). London: Bentham.

Gardner, T. N. & Kotch, M. A. 1976 A dynamic analysis of riser and caissons by the finite element method. In *Proc. of the 1976 Offshore Technology Conf.* (Houston, TX), paper no. OTC 2651.

Horton, E. 1975 Tension leg platform prototype completes Pacific coast test. *Ocean Industry*, September issue, 245–247.

Jefferys, E. R. & Patel, M. H. 1982 Dynamic analysis models of the tension leg platform. *J. Energy Resources Technol.* **104**, 217–223.

Jefferys, E. R. & Rainey, R. C. T. 1994 Slender body models of TLP and GBS ringing. In *7th Behaviour of Offshore Structures, BOSS'94* (ed. C. Chryssostomidis), vol 2, pp. 587–605. Oxford: Pergamon.

Kitami, E., Ninomiya, M., Katayama, M. & Unoki, K. 1982 Response characteristics of tension leg platform with mechanical damping systems in waves. In *Proc. 14th Offshore Technology Conf.* (Houston, TX), paper no. OTC 4393.

Lonergen, J. E. 1979 Development of Seafox tethered buoyant platforms. In *Proc. Symp. on New Technologies For Exploration of Oil and Gas Resources' Commission of the European Communities* (Luxembourg), pp. 970–994.

Lonergen, J. E. 1980 Dynamic behaviour of models of tethered buoyant platforms. In *Proc. European Offshore Petroleum Conf. and Exhibition* (London), paper no. EUR 265, pp. 535–544.

MacDonald, R. D. 1974 The design and field testing of the 'Triton' tension leg fixed platform and its future application for petroleum production and processing in deep water. In *Proc. 6th Offshore Conf.* (Houston, TX), paper no. OTC 2104.

Malahy, R. C. 1986 A non-linear finite element method of the analysis of offshore pipelines, risers and cable structures. In *Proc. of the 1986 Offshore Mechanics and Arctic Engineering Symp. ASME* (Tokyo).

McIver, D. B. & Lunn, T. S. 1983 Improvements to frequency domain riser programs. *Proc. of the 1983 Offshore Technology Conf.* (Houston, TX), paper no. OTC 4550.

Mercier, J. A. 1982 Evolution of tension leg platform technology. Presented at *Third Int. Conf. on the Behaviour of Offshore Structures* (MIT).

Miller, J. E. & Young, R. D. 1985 Influence of mud column dynamics on top tension of suspended deepwater drilling risers. In *Proc. of the Offshore Technology Conf.* (Houston, TX), paper no. OTC 5015.

Morgan, G. W. 1976 Applied mechanics of marine riser systems. *Petroleum Engineer* parts 1–3, October 1974 to May 1976.

Natvig, B. J. & Pendered, J. W. 1977 Nonlinear motion response of floating structures to wave excitation. In *Offshore Technology Conf.*, paper no. OTC 2796.

Patel, M. H. & Lynch E. J. 1983 The coupled dynamics of tensioned buoyant platforms and mooring tethers. *J. Engng Struct.* **5**, 299–308.

Patel, M. H. & Park, H. I. 1992 Comparative evaluation of tension leg platforms with reduced tether tensions. in *Proc. the Behaviour of Offshore Structures Conf., BOSS 92* (Imperial College, 7–10 July) pp. 599–616. London: Bentham.

Patel, M. H., Sarohia, S. & Ng, K. F. 1984 Finite element analysis of the marine riser. *J. Engng Struct.* **6**, 161–170.

Paulling, J. R. & Horton 1970 Analysis of the tension leg platform, OTC 1263. In *Proc. 1st Offshore Technology Conf.* (Houston, TX), paper no. OTC 1263.

Perrett, G. R. & Webb, R. M. 1980 Tethered buoyant platform production system. In *Proc. 12th Offshore Technology Conf.* (Houston, TX), paper no. OTC 3881.

Rainey, R. C. T. & Smith, S. 1993 Application of slender body theory and accurate wave kinematics to ringing calculations: a critique of the Morison–Wheeler methodology. In *Proc. of the Seminar on Tension Buoyant Platforms* (ed. M. H. Patel). Lonon: Bentham.

Robren, E. M. Q. & Steinsvik, B. 1978 Deep water resonance problems in the mooring system of the tethered platform. In *Proc. Int. Conf. on Offshore Structures Engineering* (Rio de Janeiro).

Seyed, F. B. & Patel, M. H. 1992 Mathematics of flexible risers including pressure and internal flow effects. *Marine Struct.* **5**, 121–150.

Sparks, C. P. 1979 Mechanical behaviour of marine risers mode of influence of principal parameters. In *Proc. of the Winter Annual Meeting of the American Society of Mechanical Engineers 7* (New York, 2–7 December).

PHILOSOPHICAL TRANSACTIONS OF THE ROYAL SOCIETY A MATHEMATICAL, PHYSICAL & ENGINEERING SCIENCES

Sparks, C. P., Cabillic, J. P. & Schawann, J. C. 1983 Longitudinal resonant behaviour of very deep water risers. In *Proc. 1983 Offshore Technology Conf.* (Houston, TX), paper no. OTC 4317.

Tassini, P. & Panuzzola, A. 1981 A tension leg platform for 100 m water depth. In *Proc. Deep Offshore Technology Conf.* (Palma de Mallorca, October), vol. II, paper no. 11.2.1.b., pp. 155–162.

Wang, E. 1983 Analysis of two 13200 ft riser systems using a three dimensional riser program. In *Proc. 1983 Offshore Technology Conf.* (Houston, TX), paper no. OTC 4563.

Young, R. D. & Fowler, O. O. 1978 Mathematics of marine risers. In *The Energy Technology Conf. and Exhibition* (Houston, TX).

Received 1 May 1995; revised 22 August 1995; accepted 26 September 1995

PHILOSOPHICAL TRANSACTIONS OF THE ROYAL SOCIETY A MATHEMATICAL, PHYSICAL & ENGINEERING SCIENCES